CHALMERS
UNIVERSITY OF TECHNOLOGY

Spin Dependent Discrimination between Majorana and Dirac Dark Matter

Master's thesis in Physics and Astronomy

Erik Johansson

Department of Physics
CHALMERS UNIVERSITY OF TECHNOLOGY
Gothenburg, Sweden 2019

Master's thesis 2019

Spin Dependent Discrimination between Majorana and Dirac Dark Matter

ERIK JOHANSSON

CHALMERS
UNIVERSITY OF TECHNOLOGY

Department of Physics
Division of Subatomic and Plasma Physics
Chalmers University of Technology
Gothenburg, Sweden 2019

Spin Dependent Discrimination between Majorana and Dirac Dark Matter
ERIK JOHANSSON

Supervisor: Riccardo Catena, Assistant Professor, Department of Physics
Examiner: Gabriele Ferretti, Professor, Department of Physics

Master's Thesis 2019
Department of Physics
Division of Subatomic and Plasma Physics
Chalmers University of Technology
SE-412 96 Gothenburg
Telephone +46 31 772 1000

Typeset in LaTeX
Gothenburg, Sweden 2019

Spin Dependent Discrimination between Majorana and Dirac Dark Matter
ERIK JOHANSSON
Department of Physics
Chalmers University of Technology

Abstract

A large number of observations reveal deviations from expected gravitational behaviour in astrophysical systems. This suggests that something is missing in our understanding of the Universe. A well established candidate for explaining these deviations is dark matter, a kind of matter that is not subject to photon interactions and thus can not be detected by absorbed or emitted light - it is dark. Even though we can not observe it at any detectable wavelength, dark matter is postulated to interact via gravitation. These interactions would then account for the shortcoming of gravitational pull from visible mass, explaining the observed irregular gravitational behaviour. One leading hypothesis is that the proposed dark matter component of the Universe is actually made out of massive, weakly interacting particles. As of today, there has not yet been any detection of such a particle, leaving the fundamental properties of dark matter unknown.

There are currently several ongoing experimental projects searching for dark matter particles, and more are being planned. Furthermore, their accuracy is higher than ever, and if the dark matter particle hypothesis is correct, it is reasonable to expect a detection signal in the foreseeable future. The different searches take complementary approaches and exploit either annihilation, production or direct detection experiments. The latter, which is the focus of this thesis, aims to detect dark matter by measuring the recoil of a target nucleus in a detector when a dark matter particle scatters off of it. In case of positive detection at direct detection experiments, a model describing the interaction between dark matter particles and baryonic matter is needed in order to be able to draw conclusions about the dark matter particle properties.

Under the assumption that dark matter is a spin 1/2 particle that only interacts with baryonic matter via spin dependent interactions, this thesis studies dark matter-nucleus scattering in order to see if it is feasible to discriminate between Majorana and Dirac dark matter. I find that, if dark matter particles are detected at three different experiments, the Majorana dark matter hypothesis can be rejected in favour of an alternative hypothesis in which dark matter is a Dirac particle. Restrictions on target elements that are of interest for this test are presented, and the test procedure is studied for setups containing some of them, namely: ^{131}Xe, ^{127}I, ^{73}Ge, ^{23}Na and ^{19}F.

Keywords: dark matter, direct detection, nucleus scattering, Dirac, Majorana.

Acknowledgements

First and foremost I would like to thank my supervisor Riccardo Catena, both for the opportunity to do this project and for the helpful support, countless discussions and the feedback that he has provided. It has been a pleasure working together.
A large thank you is also in place for the rest of our dark matter group, consisting of Julia Ravanis, Timon Emken and Vanessa Zema. Thank you for interesting group meetings and fruitful discussions about our projects. Your support and input has helped me a lot when working on this thesis.

Erik Johansson, Gothenburg, June 2019

Contents

1
Introduction

Reaching several decades back in time, there are large amounts of observations that show unexpected gravitational effects in astrophysical and cosmological systems [1]. These observations study phenomena at sizes starting from the width of galaxy clusters, reaching all the way up to cosmological scales. They all have one thing in common; they end up implying the need for gravitational forces that can not be accounted for by the observable mass in the systems. In order to make sense out of this, it is today widely accepted that there should be some kind of invisible mass in the Universe that does not interact with photons, i.e. that can not be seen by observing its absorption or emission of light. This hypothetical invisible mass is what is called dark matter.

Even though so many different observations hints at the existence of dark matter, there has still been no direct verification of its existence. Characterising dark matter is crucial, and is one of the most urgent problems in modern physics, being placed high on the lists of future research goals in astroparticle physics (see e.g. [2]). One of the reasons for this is the possible implications a detection of dark matter particles would have for the Standard Model, as a dark matter particle would require an extension of it. Assuming that such a particle exists, in order to obtain any theoretical predictions, specific models of dark matter are studied to try to predict what a dark matter discovery might look like in terms of physical observables. Typical physical observables include rates of dark matter-nucleus scattering events in low-background experiments located deep underground, and fluxes of dark matter annihilation products produced in dark matter dominated astrophysical systems. If one of these signals is detected, one could then compare the theoretical models with actual measurements and from there begin to establish the particle nature of dark matter.

In this thesis, dark matter is assumed to be a spin 1/2 particle, meaning that it will be a fermion. As the dark matter particle is massive, this choice implies that dark matter can be either a Dirac or a Majorana fermion, where the latter would mean that dark matter would constitute its own antiparticle. The aim is to study the physical observables of scattering experiments, where a dark matter particle scatters off a target nucleus, and see how these observables can be used to discriminate between Majorana and Dirac dark matter. The discrimination procedure that is presented here is based on a study published by Kavanagh et al. [3], in which they focus on so called spin independent dark matter-nucleon interactions as underlying dark matter interaction theory. They found that in certain cases, it should in principle be possible to use scattering experiments to conclude that the dark matter particle is a Dirac particle, given that experimental measurements of

dark matter scattering have occurred. In this thesis, we instead consider an alternative theoretical framework, so called spin dependent interaction theory, in order to investigate if a corresponding conclusion can be made.

Due to the velocity of incoming dark matter particles arriving at the Earth being low, the scattering takes place in a non-relativistic setting. My starting point for calculating the relevant cross sections is however a relativistic Lagrangian, describing the interactions of dark matter and nucleons. I start by expanding the relativistic nucleon interactions in their low velocity limit in order to find the non-relativistic theory. These non-relativistic nucleon interactions are then used to construct a corresponding nucleus description. The mapping from nucleons to nucleus is done via form factor calculations. The central quantity when studying the scattering is the cross section for dark matter-nucleus scattering, which then can be converted into an event rate for a given detector. Given that a certain amount of measurements take place, it should then be possible to use the collected data to analyse the particle nature of dark matter particles. I conclude my calculations by describing how the choice of experimental targets suitable for discrimination is made, based on the underlying interaction theory.

In chapter 2, background information on the dark matter problem is presented. This includes a brief historical review, astrophysical phenomena that can be explained by introducing dark matter, different candidates and the outline for experimental searches for verification of its existence. Chapter 3 covers the fundamental theory needed to study dark matter-nucleus scattering, such as spinor conventions, field theory, scattering theory and cross sections. The test procedure for discriminating between Dirac and Majorana dark matter is outlined in chapter 4. This includes limitations on under what circumstances the test works, as well as what target elements that can be used for discrimination. Numerical tools and a suggestion for a statistical procedure suitable for finding the discrimination significance of the test results are also covered in this chapter. A measure of how suitable the targets found in chapter 3 are for discrimination is presented in chapter 5. These results and the choice of targets are discussed in chapter 6. A concluding summary of the results and their implications, as well as a few suggestions on extensions of the study, is presented in chapter 7.

2

Dark matter

This section contains a summary of astrophysical observations that supports the dark matter hypothesis. The scales where these observations are made range from galactic all the way up to cosmological sizes. Some of the top candidates for dark matter are mentioned and discussed in short. We also outline the main three experimental approaches to confirming the existence of a dark matter particle, with focus on direct detection, as this is the main observational method of relevance to this thesis.

2.1 Evidence for dark matter

The historical background of dark matter is tightly bound together with the history of our exploration of the Universe. Even though the pioneers of astrophysics, such as Galileo Galilei, helped us reach the amount of knowledge that we have today, it was possibly Friederich Bessel who was the first to infer the existence of an object based solely on its gravitational effects [1, 4]. The first insight about the presence of invisible mass in the Universe arose from the graviational pull of stars that, by then, were out of observational reach. Even though this was in no way connected to dark matter per se, his way of thinking about the source of gravitational effects would later lead the pioneers of dark matter to their findings. This created the theoretical framework of dark matter theory, which is still used today when trying to verify its existence. From this starting point, a large set of different observed indicators of dark matter have been found, and now we will have a look at some of the most important ones.

2.1.1 Galaxy clusters

The first example of observations that supports the existence of dark matter appears on the galactic scale. In 1933, Fritz Zwicky noticed large deviations in apparent velocities of several galaxies in the Coma Cluster, which lead him to examine the expected mass content and velocity dispersion of the cluster [1, 5, 6]. Using the viral theorem to infer expected mass and corresponding velocity dispersion, he found that there was a much larger velocity dispersion than what was expected from the observed luminous mass in the cluster.

The viral theorem for a stable, non-accelerating galaxy cluster can be written in terms of the average kinetic energy E_{kin} and total gravitational energy E_{tot} of the

system as

$$2E_{\text{kin}} + E_{\text{tot}} = 0. \tag{2.1}$$

Substituting the specific galactic quantities in E_{kin} and E_{tot}, we get

$$2\frac{M\langle v^2\rangle}{2} - \frac{1}{2}\frac{GM^2}{R} = 0, \tag{2.2}$$

where the quantities used are the galaxy mass M, the average velocity squared $\langle v^2\rangle$, the gravitational constant G and R, the typical separation between galaxies in the cluster (which gives a measure of the size of the cluster). Solving for the velocity dispersion of a single galaxy, we arrive at

$$\langle v^2\rangle = \frac{MG}{2R}. \tag{2.3}$$

Assuming 800 observed galaxies in the Coma cluster, $M = 10^9$ solar masses and that the cluster was contained within a sphere of radius 10^6 light years, Zwicky concluded that the velocity dispersion should be about 80 km/s for the Coma cluster. However, the observed value was of the order of 1000 km/s [1]. This implies that there is more mass present in the Coma cluster than what is observed, leading to the first of many hints of the presence of dark matter in the Universe. Worth noting is that there are today several more accurate ways to determine the mass of a galaxy cluster, e.g. by gravitational lensing (see [7] for an example), but the problem with the missing luminous mass remains.

2.1.2 Galactic rotation curves

Further measurements on galactic scales were carried out during the twentieth century. During this period, rotation curves, the tangential velocity of galaxy content as a function of distance from the galactic centre, were made for a wide range of galaxies [8, 9, 10]. Conclusions based on these rotation curves started to emerge within the scientific community sometime around 1970 [1]. The idea is based on that, under the assumption of a spherically symmetric galaxy, the centrifugal force F_{cent} and gravitational force F_{grav} in a stable rotating galaxy cancel each other out. This gives the relation

$$F_{\text{grav}} - F_{\text{cent}} = 0. \tag{2.4}$$

An enclosed volume of mass m, rotating around the galactic centre at a distance r with velocity v, will be subjected to a centrifugal force

$$F_{\text{cent}} = \frac{mv^2}{r}. \tag{2.5}$$

The gravitational force acting on the same volume of mass m is

$$F_{\text{grav}} = \frac{GmM}{r^2}, \tag{2.6}$$

where M is the mass enclosed in the whole sphere of radius r around the galactic centre. As per equation (2.4), we then get that the velocity scales as

$$v(r) = \sqrt{\frac{GM}{r}} \propto r^{-1/2}. \tag{2.7}$$

This scaling is valid for constant M only, meaning that it should hold for large values of r, when we are far away from the massive galactic centre. The interpretation of this result is that the velocity of chunks of mass should fall of at large distances from the galactic centre, where most observable mass is located. However, rotation curves has been made for many different galaxies, and they do not follow the expected behaviour at all. An example of a rotation curve is presented in Figure 2.1, for the spiral galaxy Messier 33. It is there apparent that the circular velocity is approximately constant (or slightly increases) for large galactocentric distances, and that it does not scale as $r^{-1/2}$. Observations of this kind suggests that something is missing in the current knowledge about gravitational phenomena within our galaxy. Even though these effects are widely assumed to be due to some kind of dark matter, it is worth noting that other hypothetical explanations exists, such as different modified theories of gravity (see e.g. [11]).

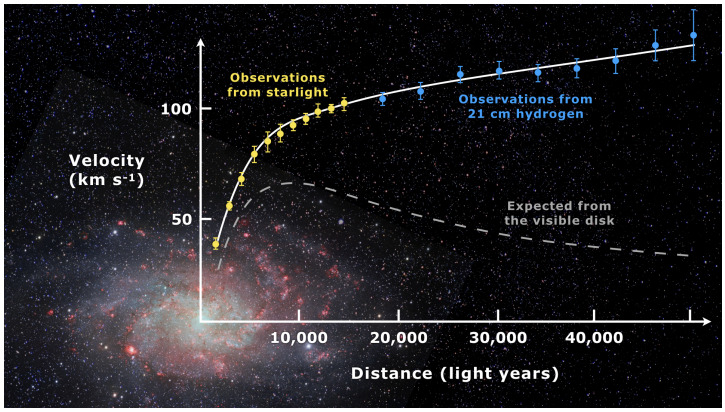

Figure 2.1: A rotation curve of the spiral galaxy Messier 33, published under public domain [12]. The flat behaviour of the circular velocity V_{cir} over large distances is seen clearly. It is here apparent how the measured velocity based on starlight and the hydrogen spectrum gives a much larger total gravitational pull than what is expected from the visible mass in the galaxy, hinting at the existence of dark matter.

2.1.3 Galaxy cluster merging

One of the strongest proofs for dark matter on the scale of galaxy clusters is supplied by the so called Bullet cluster, a system resulting from the merging of two clusters of galaxies [13, 14]. Both X-ray and weak lensing observations of the Bullet cluster have been performed. While X-ray observations provide the baryonic mass distribution in the cluster, the weak leansing technique has been used to obtain the total mass distribution in the system. The offset between the two peaks of the total mass distribution is much larger than the corresponding offset in the baryonic mass distribution, hinting at the presence of dark matter in the cluster [14]. This effect arises from the slow-down of baryonic matter inside the clusters during the collision, as ordinary matter is slowed down by scattering. The dark matter scatters weakly or not at all, meaning that the dark matter will be less subject to the collision. The difference between total gravitational mass and visible mass content then implies the existence of weakly or non-self interacting dark matter in the cluster. A picture

of the Bullet cluster, created from X-ray measurements and gravitational lensing observations, is provided in Figure 2.2.

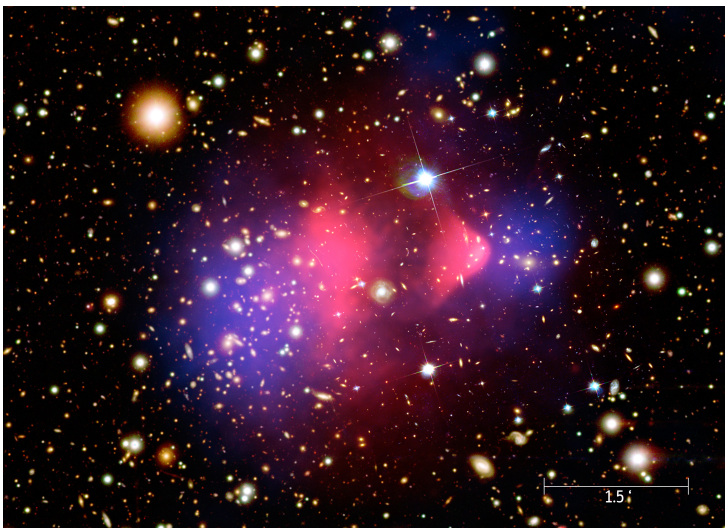

Figure 2.2: A photo of the Bullet Cluster (1E0657-56), captured by Chandra X-ray Observatory [15] and provided by NASA under public domain. The visible light-spectrum is shown, as well as the X-ray emissions (pink areas) and the mass distribution calculated via gravitaional lensing (blue areas). A size scale is given in arcmin at the bottom.

2.1.4 Cosmological scale

As measurements of galaxy properties grew in number, their implication on cosmological scales started to emerge in the minds of physicists. As a matter of fact, this was a natural next step. This is due to the fact that however good evidence the galactic scale observations make for the *existence* of dark matter, they give no information about what *amount* there is. This information can instead be accessed by looking at the cosmic microwave background, often denoted CMB [16]. In a scenario with baryonic matter only, large scale cosmological structures can form only after recombination, due to matter radiation interactions contrasting the gravitational collapse. On the other hand, in a scenario with dark matter, density fluctions can grow even before recombination since dark matter and radiation are essentially decoupled in this context. These effects can be seen in the CMB background, which will be discussed in the following section.

2.1.4.1 Cosmic Microwave Background

CMB photons are remnants from the decoupling between photons and matter in the early universe [17]. At this point, the Universe was sufficiently cool for atoms to start forming, leaving the CMB photons to travel freely ever since. Due to the expansion of the Universe, these photons have been redshifted by a certain amount, that can be concluded from the study of other astrophysical phenomena [18]. It is established that CMB is effectively described in terms of a black body radiation with temperature $T \approx 2.73$ K, mildly dependent on the observation direction.

These deviations are called anisotropies of the spectrum [19]. The anisotropies arose when the competition between attractive gravitational forces of matter and repulsive forces from photon pressure caused the baryonic matter to oscillate. Later, when the CMB photons decoupled from matter in the early Universe, information of these oscillations remained in the CMB photon density that we can observe today. However, if there exists dark matter in the Universe, the extra gravitational potential would then change these oscillations over time, resulting in observable changes in the CMB photon spectrum that can be used to justify the existence of dark matter [20]. A multipole expansion of the CMB photon spectrum is shown in Figure 2.3, where the anisotropies can be seen. It shows the angular scale dependency of the temperature anisotropies mentioned above.

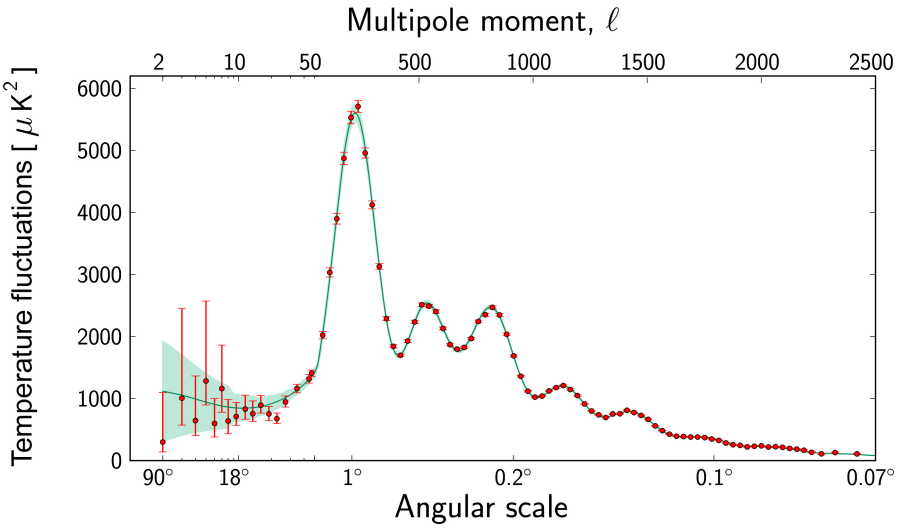

Figure 2.3: A multipole expansion of the CMB power spectrum shown as a function of its angular dependence, copyright: ESA and the Planck Collaboration [21]. The data points are CMB temperature measurements, and we can observe that they closely follow their predicted values based on different cosmological models containing dark matter, see e.g. [18, 19].

2.2 Dark matter candidates

Due to the current absence of detection of dark matter particles, the microscopic properties of dark matter remain as yet unknown. However, several dark matter candidates have been proposed in the literature. In this section some of the most extensively investigated dark matter candidates are reviewed briefly. Additional information on dark matter candidates is widely available in the literature, see for example [16, 22].

2.2.1 WIMP

Weakly Interacting Massive Particles, or WIMPs, are exactly what the name suggest, particles that have mass and interacts with baryonic matter with strength comparable to or smaller than the weak scale. Their remaining particle properties are model dependent, so the span of possible WIMP candidates is rather large. The most popular candidates for dark matter are different kinds of WIMPs. Two kinds that get a lot of attention are SUSY (supersymmetry) neutralinos and Kaluza-Klein states from extra dimensional theories. SUSY is an extension of the Standard Model, stating that all particles have supersymmetric partners with the same mass and gauge quantum numbers (as long as SUSY is an exact symmetry of Nature), but have spin differing by 1/2 (see e.g. [23]). Kaluza-Klein states arise within a unified field theory built around a fifth dimension [24]. Both photon and neutrino states that are WIMP candidates arise within the Kaluza-Klein theory. The dark matter particle studied in this thesis is assumed to be a WIMP, but we do not go more into the details of its various quantum properties apart from its particle-antiparticle nature.

Experimental searches for WIMP dark matter candidates have so far not been able to pin down any explicit WIMPs, but there are results that indirectly hints at their existence. By continuously making measurements of how the background signal in detectors on Earth is modulated over the years, the DAMA/LIBRA collaboration has published results that seem to agree with the predicted annual modulation of hypothetical dark matter signals [25]. The expected modulation of dark matter signals is due to Earth's rotation in the Milky Way, meaning that a fixed detector will have different exposure to dark matter particles depending on what time of year it is. Unfortunately, there has still been no confirmation of these results, as the experimental measurements as of today have not been successfully reproduced.

2.2.2 Sterile neutrinos

Another candidate for dark matter is a modified version of Standard Model neutrinos. They differ in the sense that they do not interact via the weak nuclear force. However, they obviously are still assumed to interact via gravitational force in order to be a viable candidate for dark matter. Dark matter cannot be made of Standard Model neutrinos, since they are relativistic during the formation of the large scale cosmological structures, in disagreement with observations [26]. A natural extension from the left-handed neutrinos of the Standard Model is then right-handed neutrinos, that would only couple to the Standard Model ones via oscillation between left- and right chirality [26]. The sterile neutrino hypothesis implies that their mass is of the order of a few keV [27].

2.2.3 Axions

Axions are hypothetical pseudoscalar particles, and have been introduced in order to resolve the strong charge-parity problem of quantum chromodynamics. If they exists, and turn out to both satisfy a fundamental set of constraints and be within a certain mass region, they are also a candidate for a dark matter particle of mass

lower than about 0.01 eV [28]. They are also thought to interact weakly with all Standard Model particle, one of the main reasons to why they are considered to be good dark matter candidates. However, experimental searches for axions have so far failed to verify their existence [29].

2.3 Experimental techniques

Experimental searches for dark matter WIMP candidates are carried out with three different approaches; indirect detection, collider experiment and direct detection. This section briefly covers each of these approaches.

2.3.1 Indirect detection

If dark matter is of particle nature, and furthermore also has a antiparticle, it should in theory be possible to measure signal due to products from the annihilation of dark matter particles in the Universe. This is what is meant by indirect detection, instead of measuring scattering events where dark matter particles are involved directly, the dark matter particles are indirectly studied by looking at the "trace" they leave in the Universe. Not only annihilation can be the source of potential indirect signals. If it turns out that the dark matter particle has a limited lifetime, its decay products are also something that could be seen as signals in detection experiments. In order for these two kind of annihilation/decay products of dark matter to be detectable in our ordinary experimental setups, they must be Standard Model members. If the decay products for instance turns out to be another kind of dark matter particle or something similar, the problem with detecting them would be the same as with dark matter. Annihilation traces of dark matter have been studied in detail (see e.g. [30]).

2.3.2 Production experiments

If dark matter is made of WIMPs, it should in principle be producible in collider experiments. For instance the ATLAS experiment at LHC at CERN could produce dark matter particles when protons collide. The LHC proton collisions has a centre of mass energy of 14 TeV [31], so dark matter particles of the order of a few TeV could in principle be created there. The effect of producing dark matter particles in current collider experiments would not be detected in interactions with the detectors themselves, but rather as missing momenta in other detectable particles. As can be seen from this brief summary, detecting dark matter this way brings along some subtleties. For instance, other light particles, such as Standard Model neutrinos, would also show themselves as missing momenta in the detector signals. As a result of this, additional experimental constraints might be needed if dark matter particles are to be discovered in this way. Finally, if a dark matter particle was to be produced and detected with high accuracy, additional experiments or other reasoning is needed in order to prove that it is actually the same Milky Way dark matter particle that we search for, and not just a new particle of another kind. It can thereby be stated

that dark matter experimental searches in collider experiments alone might not be suitable to explain dark matter phenomena in the Universe.

2.3.3 Direct detection

Under the assumption that dark matter particles interacts with ordinary matter on the weak scale, they should be detectable in experimental setups, given that they are sensible enough. Direct detection experiments aim to measure the recoil of a nucleus in a detector when a dark matter particle scatters off of it. Many detectors are today searching for signals of dark matter interactions, but as of yet no definite ones has been found. However, the results so far are still of great importance in the search for dark matter, as many of them can be used to set constraints on e.g. the possible cross section of dark matter scattering with nucleus targets [32]. The scattering recoils are expected to be of the order 1 to 10^2 keV, under the assumption that dark matter particles are WIMPs with a mass of about 10 to 10^3 GeV [33]. Due to the low interaction strength that is expected, a low or preferably zero background is of outermost importance for direct detection experiments to ever be probable to measure dark matter interaction signals [34]. This is mainly to avoid background noise from e.g. cosmic muons or other low interaction particles to reach the detector. The number of recoil events in a target nucleus can be related to the differential rate of scattering events R per recoil energy E_R. With input from astrophysical and particle physics calculations of a underlying dark matter theory, these recoil rates can then be interpreted to obtain information about the dark matter particle. Such a interpretation is made in this thesis, namely; under the assumption that a certain value for the dark matter-nucleus cross section is measured, can we conclude anything about the particle/antiparticle nature of the scattered dark matter particle? A more in-depth relation between measured events, astrophysical input and particle physics is given in the next section.

2.3.4 Direct detection event rates

The experimental direct detection search for dark matter is based on observing the recoil of a target nucleus in a detector when a dark matter particle scatters off it. The experimental observable in these experiments is the differential recoil spectrum in some energy range. For a single nucleus target A with recoil energy E_R, the expected rate of nuclear recoils per recoil energy is [34, 35]

$$\frac{dR}{dE_R} = \frac{\rho_\chi}{m_\chi m_A} \int_{v_{\min}}^{v_{\text{esc}}} v\, f(v,\, t) \frac{d\sigma_{\chi A}}{dE_R}\, \mathrm{d}v, \tag{2.8}$$

where the input parameters on the right hand side can be divided into two subcategories; one arising from astrophysical and one from particle physics calculations respectively. The astrophysical parameters are the local dark matter density in the Milky way, denoted ρ_χ, and the dark matter velocity distribution in the detector frame of reference, denoted $f(v,\, t)$. The time dependency in $f(v,\, t)$ is due to the rotation of the Earth, and is not considered in this study. From here on, the time dependency is thus dropped and the velocity distribution is written as $f(v)$. The

particle physics inputs are the two masses of the target nucleus and the incoming dark matter particle, denoted m_A and m_χ respectively, and the differential cross section $\frac{d\sigma_{\chi A}}{dE_R}$ of dark matter-nucleus scattering. The latter is the main quantity of study in this thesis, and depends entirely on the underlying theory that describes the interaction of dark matter with Standard Model particles.

2.3.5 Astrophysical input parameters

As the rest of the thesis focuses primarily on the differential cross section $\frac{d\sigma_{\chi A}}{dE_R}$, a comment on the suitable values for the astrophysical parameter input is made here. The local dark matter density ρ_χ is not a fixed quantity, but restrictions based on observational data puts it in the range 0.2-0.8 GeV cm^{-3} [36]. Letting $\rho_\chi = 0.3$ GeV cm^{-3}, as is done in e.g. [3], is thus a valid assumption. An isotropic Maxwell-Boltzmann distribution is often assumed for $f(v)$ [37], with a speed dispersion of $\sigma_v = 156$ km s^{-1} and the velocity of the Earth relative the galactic halo taken to have the constant value $v_{\text{Earth}} = 232$ km s^{-1} [38, 39, 40]. The escape velocity $v_{\text{esc}} = 544$ km s^{-1} is set according to the Milky Way local escape speed [41, 42]. The lowest possible velocity of a dark matter for it to create a recoil in target A is derived in section 3.3, and is there shown to be given by

$$v_{\min}(E_R) = \sqrt{\frac{m_A E_R}{2\mu_{\chi A}^2}}, \tag{2.9}$$

where $\mu_{\chi A}$ is the reduced mass of the dark matter-target system.

3

Theoretical framework

This section covers the conventions used in the scattering calculations as well as a review of scattering physics. Conventions regarding description of spinors, particle fields etc. are also stated. A review of Majorana and Dirac particles, as well as their differences, is presented. The interpretation of scattering events in terms of cross sections is given, as is the effective field theory (EFT) of the underlying dark matter theory. A few important calculations of relevant differences in the cross section in the case of Majorana or Dirac dark matter are also made.

3.1 Conventions

3.1.1 Units, metric and contraction

The calculations within this work are always carried out in natural units, i.e. units where

$$c = \hbar = 1. \tag{3.1}$$

The four dimensional spacetime metric is defined as

$$\eta^{\mu\nu} = \eta_{\mu\nu} = \begin{pmatrix} 1 & 0 & 0 & 0 \\ 0 & -1 & 0 & 0 \\ 0 & 0 & -1 & 0 \\ 0 & 0 & 0 & -1 \end{pmatrix}, \tag{3.2}$$

which means that the contraction of two spacetime four-vectors a^μ and b_μ is

$$a^\mu b_\mu = \eta^{\mu\nu} a_\nu b_\mu = a_0 b_0 - a_i b_i. \tag{3.3}$$

In the spatial term, as well as the rest of the thesis unless otherwise stated, the occurrence of the same index twice in a term indicates summation (Einstein summation convention). For example, in the case above we have ($i = 1, 2, 3$):

$$a_i b_i = a_1 b_1 + a_2 b_2 + a_3 b_3. \tag{3.4}$$

3.1.2 Spinor conventions

This section contains a summary of spinor conventions, mostly based on Chapter 3 of "An Introduction to Quantum Field Theory" by Peskin and Schroeder [43], and the interested reader is thus asked to turn there for a more thorough and detailed

explanation of spinors. As the dark matter particles are assumed to be of spin 1/2, their spin states can be described in terms of two component spinors in combination with Pauli matrices. The used conventions for these objects are as follows. The Pauli matrices are

$$\sigma^1 = \begin{pmatrix} 0 & 1 \\ 1 & 0 \end{pmatrix}, \quad \sigma^2 = \begin{pmatrix} 0 & -i \\ i & 0 \end{pmatrix}, \quad \sigma^3 = \begin{pmatrix} 1 & 0 \\ 0 & -1 \end{pmatrix}, \tag{3.5}$$

and will continuously be used in terms of the Pauli vector, defined as

$$\vec{\sigma} \equiv (\sigma^1, \sigma^2, \sigma^3). \tag{3.6}$$

Two useful relativistic quantities σ^μ and $\bar{\sigma}^\mu$ can be formed from $\vec{\sigma}$ as

$$\sigma^\mu \equiv (\mathbb{1}, \ \vec{\sigma}) \tag{3.7}$$

and

$$\bar{\sigma}^\mu \equiv (\mathbb{1}, \ -\vec{\sigma}) \tag{3.8}$$

respectively. The spins are defined to be aligned along the z-axis, and can be either up or down. These up and down states are represented by the two component spinors

$$\xi_0 = \begin{pmatrix} 1 \\ 0 \end{pmatrix}, \quad \xi_1 = \begin{pmatrix} 0 \\ 1 \end{pmatrix}, \tag{3.9}$$

respectively. They are normalised in such a way that

$$\xi_i \xi_j^\dagger = \xi_i^\dagger \xi_j = \delta_{ij}, \tag{3.10}$$

and

$$\xi^i \xi_i^\dagger = \mathbb{1}. \tag{3.11}$$

We are studying a scattering process involving two particles, and thereby have four different spins to keep track of. We will index incoming (outgoing) spin states with s (s') for the dark matter particle and r (r') for the nucleus. The spin operator for the dark matter (χ) and nucleus (N) can then be written

$$\vec{S}_{\chi,s,s'} = \frac{1}{2}\xi_s^\dagger \vec{\sigma} \xi_{s'}, \quad \vec{S}_{N,r,r'} = \frac{1}{2}\xi_r^\dagger \vec{\sigma} \xi_{r'}. \tag{3.12}$$

With the Pauli matrices defined in equation (3.5), the spin 1/2 represenation of the theory can be constructed in terms of the gamma matrices γ^μ. They satisfy the anticommutation relations

$$\{\gamma^\mu, \gamma^\nu\} \equiv \gamma^\mu \gamma^\nu + \gamma^\nu \gamma^\mu = 2g^{\mu\nu} \times \mathbb{1}. \tag{3.13}$$

They can be written in terms of the Pauli matrices in the so called Weyl representation given by

$$\gamma^0 = \begin{pmatrix} 0 & \mathbb{1} \\ \mathbb{1} & 0 \end{pmatrix}, \quad \gamma^i = \begin{pmatrix} 0 & \sigma^i \\ -\sigma^i & 0 \end{pmatrix}, \tag{3.14}$$

where the index $i = 1, 2, 3$ is a spatial index and $\mathbb{1}$ is the 2×2 identity matrix. In order to simplify notification, a fifth gamma matrix

$$\gamma^5 \equiv i\gamma^0\gamma^1\gamma^2\gamma^3, \tag{3.15}$$

is introduced, and in the Weyl basis it then becomes

$$\gamma^5 = \begin{pmatrix} -\mathbb{1} & 0 \\ 0 & \mathbb{1} \end{pmatrix}. \tag{3.16}$$

The gamma matrices defined here will be used when studying the Dirac equation and its solutions in the next section.

3.2 Dirac and Majorana particles

The differences between Dirac and Majorana fields will here be discussed in some detail as a reminder. This section also follows the theory presented by Peskin and Schroeder [43], and the reader unfamiliar with these concepts is once again directed there. The Dirac equation, given by

$$(i\gamma^\mu\partial_\mu - m)\,\psi(x) = 0 \tag{3.17}$$

is a general theory description for a spin 1/2 particle field with mass m. Plane-wave solutions to equation (3.17) are given as linear combinations of terms of the form

$$\psi(x) = u(p)e^{-ip\cdot x} \tag{3.18}$$

for on-shell particles, i.e. particles with momenta p such that $p^2 = m^2$. This gives equation (3.17) the form

$$(\gamma^\mu p_\mu - m)\,u(p) = 0, \tag{3.19}$$

where the solutions $u(p)$ can be expressed in terms of spin states ξ (defined in equation (3.9)) as [43]

$$u(p) = \left(\sqrt{p_\mu\sigma^\mu}\xi,\ \sqrt{p_\mu\bar{\sigma}^\mu}\xi\right), \tag{3.20}$$

where σ^μ and $\bar{\sigma}^\mu$ are defined in equations (3.7) and (3.8) respectively. In this definition, taking the square root of a matrix is meant as taking the (positive) root of each eigenvalue.

The plane-wave solutions $u(p)$ are what will be used when constructing relevant scattering quantities in the non-relativistic limit in this thesis. Solutions $\psi(x)$ to equation (3.17) that also are solutions under conjugation of its quantum numbers, denoted as $\psi(x) \to \bar{\psi}(x)$, are called Majorana solutions. Solutions which fail to fulfil this property are Dirac solutions. Extracting the particle nature corespondents to these two field solutions, we see that they describe two different kind of fermion particles:

- Majorana particles; particles that constitute their own antiparticle,
- Dirac particles; particles that are different from their antiparticle.

Investigating under what circumstances a dark matter fermion, that interacts with a target nucleus via only spin dependent interactions, can be concluded to be a Dirac particle is the aim of this thesis.

3.3 Non-relativistic scattering theory kinematics

Here we define some kinematic quantities that will prove to be useful. As dark matter-nucleus scattering is non-relativistic, we work in a framework that does not take relativistic effects into account. We denote the incoming and outgoing momentum of the dark matter particle as $\vec{p}$ and $\vec{p}'$, while the corresponding quantities for the nucleus are denoted $\vec{k}$ and $\vec{k}'$. Conservation of momentum gives

$$\vec{p} + \vec{k} = \vec{p}' + \vec{k}', \tag{3.21}$$

and the momentum transfer, or recoil momentum, $\vec{q}$ of the process can then be defined as

$$\vec{q} \equiv \vec{p}' - \vec{p} = \vec{k} - \vec{k}'. \tag{3.22}$$

The transverse velocity $\vec{v}^{\perp}$ of the system turns out to be very useful when writing down the effective theory of dark matter-nucleus scattering. It is defined in terms of the momenta as

$$\vec{v}^{\perp} \equiv \frac{\vec{p} + \vec{p}'}{2m_\chi} - \frac{\vec{k} + \vec{k}'}{2m_A}, \tag{3.23}$$

where m_χ and m_A denotes dark matter and nucleus mass respectively.

We will be looking at nucleus recoil events as functions of the recoil momentum $q = |\vec{q}|$, so a relevant question is what the lowest dark matter velocity required to get a recoil momentum q is. The target nucleus is always assumed to be at rest before the collision, so the scattering scenario can be described as in Figure 3.1. The kinetic energy E_χ of the dark matter particle before the collision is then partly transformed into the recoil energy of the nucleus, given by $E_R = \frac{q^2}{2m_A}$, and partly into the outgoing dark matter particle kinetic energy E'_χ. In terms of a energy conservation equation, we thus have

$$E_R = E_\chi - E'_\chi \iff \frac{q^2}{2m_A} = \frac{m_\chi v^2}{2} - \frac{m_\chi v'^2}{2}. \tag{3.24}$$

Momentum conservation in the same system gives us

$$\vec{p}' = \vec{p} + \vec{q}, \tag{3.25}$$

and in terms of the scattering angle α and the angle of the recoil β, the momentum conservation can be rewritten as the projection on the axis of $\alpha = 0$ and $\alpha = \frac{\pi}{2}$. Writing out the momenta $\vec{p} = m_\chi v$ and $\vec{p}' = m_\chi v'$, the two projections are

$$m_\chi v' \cos\alpha = m_\chi v - q\cos\beta, \tag{3.26}$$

$$m_\chi v' \sin\alpha = q\sin\beta. \tag{3.27}$$

Taking the square of both these momentum equations and then adding the results now gives

$$m_\chi^2 v'^2 = m_\chi^2 v^2 - 2m_\chi v q\cos\beta + q^2, \tag{3.28}$$

where we note that the scattering angle α no longer appears. Solving for $m_\chi v'^2$ gives

$$m_\chi v'^2 = \frac{m_\chi^2 v^2 - 2m_\chi v q\cos\beta + q^2}{m_\chi}. \tag{3.29}$$

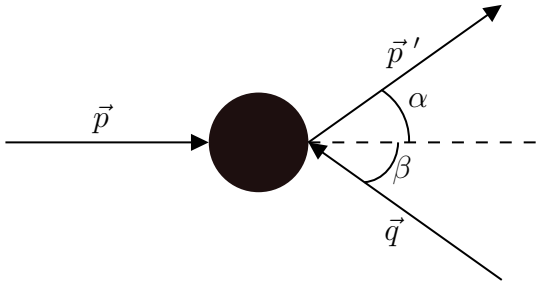

Figure 3.1: The relation of the dark matter momentum $\vec{p}$, $\vec{p}\,'$ and the nuclear recoil $\vec{q}$. The black circle represents the detailed interaction process of the scattering, and is not considered in detail here.

Putting this result back into equation (3.24) gives

$$\frac{q^2}{2m_A} = \frac{m_\chi v^2}{2} - \frac{m_\chi^2 v^2 - 2m_\chi v q\cos\beta + q^2}{2m_\chi}, \tag{3.30}$$

or equivalently

$$q\left(\frac{1}{m_A} + \frac{1}{m_\chi}\right) = 2v\cos\beta. \tag{3.31}$$

The factor of q in the left hand side of this relation is usually rewritten as the reduced mass $\mu_{\chi A}$ of the system, i.e. by introducing

$$\mu_{\chi A} \equiv \frac{m_\chi m_A}{m_\chi + m_A}, \tag{3.32}$$

so that equation (3.31) can be recast into

$$q = 2v\mu_{\chi A}\cos\beta. \tag{3.33}$$

We now have a relation for the induced recoil momentum q in direction β when an incoming dark matter particle with velocity v scatters off of a target nucleus A. The minimal velocity $v_{\min}$ for a scattering for a given q is then the value of v that equation (3.33) gives for minimal recoil angle, $\beta = 0$. We get

$$v_{\min} = \frac{q}{2\mu_{\chi A}} = \frac{\sqrt{2m_A E_R}}{2\mu_{\chi A}} = \sqrt{\frac{m_A E_R}{2\mu_{\chi A}^2}}. \tag{3.34}$$

3.4 Cross section

When studying the collision of any two particles, the quantity that describes the probability of interaction is the cross section σ. As per equation (4.79) in [43], with the same notation for incoming and outgoing particles as in section 3.3, the cross section is related to the energy, momenta and velocity of the scattered particles by the relation

$$d\sigma = \frac{1}{4E_p E_k |v_\chi - v_N|}\frac{d^3p'\, d^3k'}{4(2\pi)^2 E_{p'} E_{k'}}|\overline{\mathcal{M}}|^2\delta^{(4)}\left(p + k - p' - k'\right). \tag{3.35}$$

Here, the amplitude $\overline{\mathcal{M}}$ is a quantity calculated from coupling strength and interaction rules of the underlying particle theory, by summing over final spin states and averaging over initial spin states [43]. The amplitude for the dark matter-nucleus scatterings relevant for this thesis will be constructed in the sections following this one, starting from the nucleon level theory.

3.5 Nucleon effective field theory

When treating dark matter interactions with targets in a detector on Earth, we will work within an effective field theory. An effective field theory is a simplified reduction of a more complicated theory, but usually work to high accuracy in relevant applications. In the context of dark matter scattering, the effective field theory approach is to treat the scattering as a non-relativistic event. The justification of this comes from the fact that the hypothetical dark matter particle masses treated here are large in comparison to their assumed velocity [44]. It turns out, that in order to respect underlying fundamental symmetries, e.g. Galilean invariance, there exists a set of quantities that are the only ones that can be present in the Hermitian operators ($\mathcal{O}_\chi$ and $\mathcal{O}_N$) forming the interaction Lagrangian of the theory (see equation (3.37) below). They are given by [44]

$$\mathbb{1}_\chi,\ \mathbb{1}_N,\ i\vec{q},\ \vec{v}^{\perp},\ \vec{S}_\chi,\ \vec{S}_N, \tag{3.36}$$

and have been defined in sections 3.3 and 3.1.2. Assuming elastic scattering only, the non-relativistic contact form of the Lagrangian density is given by [45]

$$\mathcal{L}_{\text{int}} = \sum_{i=1}^{K} \alpha_i\, \bar{\psi}_\chi \mathcal{O}_\chi \psi_\chi \bar{\psi}_N \mathcal{O}_N \psi_N, \tag{3.37}$$

where $\psi_{\chi/N}$ are the non-relativistic fields corresponding to the dark matter/nucleon respectively and we have K terms in the Lagrangian, containing the operators $\mathcal{O}_\chi$ and $\mathcal{O}_N$ mentioned above. They include terms up to and including second order in the momenta $\vec{q}$, are Hermitian and can be constructed entirely from the Hermitian quantities listed in equation (3.36). When constructing the Galilean-invariant amplitude needed to link the effective field theory to experimental observables, there exists a number of operators $\mathcal{O}_i$ that are formed from $\mathcal{O}_\chi$ and $\mathcal{O}_N$. This amplitude is given by

$$\mathcal{M} = \sum_{i=1}^{N} \left(c_i^{(n)} \mathcal{O}_i + c_i^{(p)} \mathcal{O}_i \right), \tag{3.38}$$

where the number of operators N depends on the underlying particle physics model, and the coupling coefficients c_i for neutron and proton operators can be different from each other. The 15 operators $\mathcal{O}_i$ that are relevant for leading order (in momenta) scattering are gathered in Table 3.1. By labelling the nucleons by their isospin $\tau = 0, 1$ instead of the label $\alpha = p, n$, which often is more convenient when treating nucleus interactions, the amplitude in equation (3.38) can be recast into the form [45]

$$\mathcal{M} = \sum_{i}^{15} \left(c_i^0 \mathbb{1} + c_i^1 \tau_3 \right) \mathcal{O}_i = \sum_{\tau=0,\,1} \sum_{i=1}^{15} c_i^\tau \mathcal{O}_i t^\tau, \tag{3.39}$$

where the isospin operators $t^0 \equiv \mathbb{1}$ and $t^1 \equiv \tau_3$ have been introduced. Another isospin operator

$$\tau_3 \equiv \begin{pmatrix} 1 & 0 \\ 0 & -1 \end{pmatrix} \tag{3.40}$$

and two new isospin couplings

$$c_i^0 \equiv \frac{1}{2}\left(c_i^p + c_i^n\right), \qquad c_i^1 \equiv \frac{1}{2}\left(c_i^p - c_i^n\right) \tag{3.41}$$

have also been introduced. At this point, we then have an effective field theory that can be used to describe the interaction between free nucleons and dark matter particles. However, in the end we are interested in describing the recoils in dark matter-nucleus scattering. We thus have to find a way to construct dark matter-nucleus interaction theory from the dark matter-nucleon interaction theory.

$\mathcal{O}_1 = \mathbb{1}_\chi \mathbb{1}_N$	$\mathcal{O}_9 = i\vec{S}_\chi \cdot \left(\vec{S}_N \times \frac{\vec{q}}{m_N}\right)$
$\mathcal{O}_2 = \left(\vec{v}^\perp\right)^2$	$\mathcal{O}_{10} = i\vec{S}_N \cdot \frac{\vec{q}}{m_N}$
$\mathcal{O}_3 = i\vec{S}_N \cdot \left(\frac{\vec{q}}{m_N} \times \vec{v}^\perp\right)$	$\mathcal{O}_{11} = i\vec{S}_\chi \cdot \frac{\vec{q}}{m_N}$
$\mathcal{O}_4 = \vec{S}_\chi \cdot \vec{S}_N$	$\mathcal{O}_{12} = \vec{S}_\chi \cdot \left(\vec{S}_N \times \vec{v}^\perp\right)$
$\mathcal{O}_5 = i\vec{S}_\chi \cdot \left(\frac{\vec{q}}{m_N} \times \vec{v}^\perp\right)$	$\mathcal{O}_{13} = i\left(\vec{S}_\chi \cdot \vec{v}^\perp\right)\left(\vec{S}_N \cdot \frac{\vec{q}}{m_N}\right)$
$\mathcal{O}_6 = \left(\vec{S}_\chi \cdot \frac{\vec{q}}{m_N}\right)\left(\vec{S}_N \cdot \frac{\vec{q}}{m_N}\right)$	$\mathcal{O}_{14} = i\left(\vec{S}_N \cdot \vec{v}^\perp\right)\left(\vec{S}_\chi \cdot \frac{\vec{q}}{m_N}\right)$
$\mathcal{O}_7 = \vec{S}_N \cdot \vec{v}^\perp$	$\mathcal{O}_{15} = -\left(\vec{S}_\chi \cdot \frac{\vec{q}}{m_N}\right)\left[\left(\vec{S}_N \times \vec{v}^\perp\right) \cdot \frac{\vec{q}}{m_N}\right]$
$\mathcal{O}_8 = \vec{S}_\chi \cdot \vec{v}^\perp$	

Table 3.1: A summary of non-relativistic effective field theory operators that appear in dark matter-nucleon scattering amplitudes, up to second order in the recoil momenta $\vec{q}$.

3.6 Dark matter-nucleus amplitude from nucleon theory

In this work, nucleus interactions are described as the summed up interactions of the individual nucleons in the nucleus. Mapping from nucleons to a nucleus means that the nucleon amplitude in equation (3.38) has to be embedded into the description of the nucleus. This will in practice boil down to a convolution of the operators $\mathcal{O}_i$ defined in Table 3.1, where the convolution is done using spherical harmonic expansions of angular and radial plane wave operators of the individual nucleons. The description of the exact details of this convolution are omitted here for the sake of readability, and only the main results presently needed are stated. A full description of the convolution of the operators is found in [45]. Moving from one nucleon to a nucleus means that the isospin interaction described in equation (3.39) is converted to a sum over all A nucleons in the nucleus:

$$\sum_{\tau=0,\,1}\sum_{i=1}^{15} c_i^\tau \mathcal{O}_i t^\tau \rightarrow \sum_{\tau=0,\,1}\sum_{i=1}^{15} c_i^\tau \sum_{j=1}^{A} \mathcal{O}_i(j) t^\tau(j). \tag{3.42}$$

The operators $\mathcal{O}_i(j)$ are the same ones as the ones listed in Table 3.1, but for the specific nucleon j and with N now denoting the nucleus. The mass m_N remain the nucleon mass. The building blocks $\vec{S}_i$ and $\vec{q}$ are straight forward to replace for the nucleus, but the transverse velocity operator $\vec{v}^{\perp}$ now represents a set of A internal dark matter-nucleon transverse velocities, see [45] for a discussion regarding this quantity. The new interactions given in equation (3.42) allows us to write the dark matter-nucleus scattering amplitude $\mathcal{M}$ as

$$\mathcal{M} = \sum_{\tau=0,1} \sum_{i=1}^{15} c_i^{\tau} \sum_{j=1}^{A} \mathcal{O}_i(j) t^{\tau}(j). \tag{3.43}$$

The effective scattering amplitude for dark matter-nucleus interactions, $\overline{\mathcal{M}}$, is given by summing and averaging the nucleus amplitude $\mathcal{M}$ over possible combinations of the dark matter (nucleus) spins J_χ (J_A) as [45]

$$\begin{aligned} \overline{\mathcal{M}} &= \frac{1}{2J_\chi + 1} \frac{1}{2J_A + 1} \sum_{\text{spins}} |\mathcal{M}|^2 = \\ &= \sum_k \sum_{\tau=0,1} \sum_{\tau'=0,1} R_k^{\tau\tau'} \left(\vec{v}^{\perp\,2}, \frac{\vec{q}^{\,2}}{m_A^2}, \left\{ c_i^{\tau} c_j^{\tau'} \right\} \right) W_k^{\tau\tau'}(y), \end{aligned} \tag{3.44}$$

where a few new quantities have been introduced to make the reasoning a little more transparent. Writing the amplitude in this way factorises out the particle and nuclear physics into the dark matter response functions $R_k^{\tau\tau'}$ and the nuclear response functions $W_k^{\tau\tau'}$ respectively. The dimensionless variable $y \equiv (qb/2)^2$, where b is the nuclear size of the target, has also been introduced. The response functions $R_k^{\tau\tau'}$ and form factors $W_k^{\tau\tau'}$ have been studied in detail for relevant nucleus targets in many publications (see e.g. [45, 46]). All collisions studied within this thesis are assumed to take place at zero momentum transfer, i.e. in the limit $q \to 0$. This means that $R_k^{\tau\tau'}$ and $W_k^{\tau\tau'}$ both will be treated without dependence on q, as they in this case have constant values [45].

As per equation (3.44), knowing the values of $R_k^{\tau\tau'}$ and $W_k^{\tau\tau'}$ for a specific dark matter-nucleus combination is enough to be able to construct the average amplitude, and thus also the cross section. There are many advantages of using an effective field theory when studying dark matter particle interactions with target nuclei, and the biggest one is probably the fact that most high energy-models of dark matter behave in the same way in the scattering regime, meaning that they can be treated within the same effective field theory framework. We are now ready to have a look at the field theory description used in this thesis, and calculate its dark matter-nucleus cross section.

3.7 Dark matter-nucleon relativistic field theory

Having introduced how differential cross sections for dark matter-nucleus scattering can be computed in general, let us now formulate the specific theory upon which this thesis is based. The starting point of my investigation is a relativistic effective theory for dark matter-nucleon interactions. For fermionic dark matter scattering in the

zero momentum transfer limit, the most general relativistic interaction Lagrangian with nucleons is given by [47]

$$\begin{aligned}\mathcal{L} = &\lambda_{N,e}\bar{\psi}_\chi\psi_\chi\bar{\psi}_N\psi_N + \lambda_{N,o}\bar{\psi}_\chi\gamma_\mu\psi_\chi\bar{\psi}_N\gamma^\mu\psi_N + \\ &+ \xi_{N,e}\bar{\psi}_\chi\gamma_5\gamma_\mu\psi_\chi\bar{\psi}_N\gamma_5\gamma^\mu\psi_N - \frac{1}{2}\xi_{N,o}\bar{\psi}_\chi\sigma_{\mu\nu}\psi_\chi\bar{\psi}_N\sigma^{\mu\nu}\psi_N,\end{aligned} \tag{3.45}$$

where the first two terms are spin independent and the last two are spin dependent. The first two terms constitutes the Lagrangian studied by Kavanagh et al. [3], and the last two will be studied here. The Lagrangian of consideration is thus

$$\mathcal{L}_{\text{SD}} = \xi_{N,e}\bar{\psi}_\chi\gamma_5\gamma_\mu\psi_\chi\bar{\psi}_N\gamma_5\gamma^\mu\psi_N - \frac{1}{2}\xi_{N,o}\bar{\psi}_\chi\sigma_{\mu\nu}\psi_\chi\bar{\psi}_N\sigma^{\mu\nu}\psi_N. \tag{3.46}$$

As in equation (3.37), $\psi_{\chi/N}$ denotes dark matter and nucleon fields respectively. However, the theory is here presented in a relativistic setting. The four couplings $\lambda_{N,e/o}$ and $\xi_{N,e/o}$ denotes if the corresponding terms are even or odd under the conjugation $\psi_{\chi/N} \leftrightarrow \bar{\psi}_{\chi/N}$. Only the terms with couplings $\lambda_{N,e}$ and $\xi_{N,e}$ are possibly non-zero for a Majorana particle, while Dirac particles can have all four kind of terms.

3.8 Dark matter-nucleus (non-relativistic) effective field theory and amplitude

As we saw in section 3.5, the relativistic interaction Lagrangian

$$\mathcal{L}_{\text{SD}} = \xi_{N,e}\bar{\psi}_\chi\gamma_5\gamma_\mu\psi_\chi\bar{\psi}_N\gamma_5\gamma^\mu\psi_N - \frac{1}{2}\xi_{N,o}\bar{\psi}_\chi\sigma_{\mu\nu}\psi_\chi\bar{\psi}_N\sigma^{\mu\nu}\psi_N \tag{3.47}$$

will have a non-relativistic interaction Lagrangian of the form

$$\mathcal{L}_{\text{int}} = \sum_{i=1}^{K}\alpha_i\,\bar{\psi}_\chi\mathcal{O}_\chi\psi_\chi\bar{\psi}_N\mathcal{O}_N\psi_N. \tag{3.48}$$

We are interested in the differential cross section of the non-relativistic scattering of dark matter particles with target nucleus. The cross section depends on the square of the amplitude $\overline{\mathcal{M}}$ (see equation (3.35)), which we will now calculate for the spin dependent theory considered here. This is done by expanding the solutions $u(p)$ to the Dirac equation, given in equation (3.20), in the non-relativistic limit to first order in three momenta $\vec{p}$:

$$u^s(p) = \begin{pmatrix}\sqrt{p_\mu\sigma^\mu}\xi^s \\ \sqrt{p_\mu\bar{\sigma}^\mu}\xi^s\end{pmatrix} \approx \frac{1}{\sqrt{4m}}\begin{pmatrix}(2m - \vec{p}\cdot\vec{\sigma})\,\xi^s \\ (2m + \vec{p}\cdot\vec{\sigma})\,\xi^s\end{pmatrix} + \mathcal{O}(\vec{p}^2), \tag{3.49}$$

where we also have introduced the spin s of the particle described by the field solution. The conjugated field solution is then given by

$$\bar{u}^s(p) \equiv (u^s(p))^\dagger\gamma^0 \approx \frac{1}{\sqrt{4m}}\left(\xi^{s\,\dagger}\,(2m + \vec{p}\cdot\vec{\sigma})\,,\ \xi^{s\,\dagger}\,(2m - \vec{p}\cdot\vec{\sigma})\right) + \mathcal{O}(\vec{p}^2). \tag{3.50}$$

All fields $\psi_{\chi/N}$ will be expressed in this non-relativistic limit, meaning that the non-relativistic amplitude will be constructed in terms of bilinears of the forms

$$\bar{u}^{s'}(p')\gamma_5\gamma^\mu u^s(p) \tag{3.51}$$

and

$$\bar{u}^{s'}(p')\sigma^{\mu\nu}u^s(p). \tag{3.52}$$

These bilinears can be expanded in the non-relativistic limit. For the first one, this gives

$$\begin{aligned}
&\bar{u}^{s'}(p')\gamma_5\gamma^\mu u^s(p) \approx \\
&\approx \frac{1}{4m}\left(\xi^{s'\dagger}\left(2m+\vec{p}'\cdot\vec{\sigma}\right),\ \xi^{s'\dagger}\left(2m-\vec{p}'\cdot\vec{\sigma}\right)\right)\begin{pmatrix}0 & -\sigma^\mu\\ \bar{\sigma}^\mu & 0\end{pmatrix}\begin{pmatrix}\left(2m-\vec{p}\cdot\vec{\sigma}\right)\xi^s\\ \left(2m+\vec{p}\cdot\vec{\sigma}\right)\xi^s\end{pmatrix} = \\
&= \frac{1}{4m}\left(\xi^{s'\dagger}\left(2m+\vec{p}'\cdot\vec{\sigma}\right),\ \xi^{s'\dagger}\left(2m-\vec{p}'\cdot\vec{\sigma}\right)\right)\begin{pmatrix}-\sigma^\mu\left(2m+\vec{p}\cdot\vec{\sigma}\right)\xi^s\\ \bar{\sigma}^\mu\left(2m+\vec{p}\cdot\vec{\sigma}\right)\xi^s\end{pmatrix}.
\end{aligned} \tag{3.53}$$

Keeping only first order terms of $\vec{p}$, we then have

$$\bar{u}^{s'}(p')\gamma_5\gamma^\mu u^s(p) \approx \frac{1}{4m}\left[\left(4m\xi^{s'\dagger}(\vec{p}'+\vec{p})\cdot\vec{\sigma}\xi^s\right)\mathbb{1} + 8m^2\xi^{s'\dagger}\vec{\sigma}\xi^s\right], \tag{3.54}$$

which we from now on will write as a matrix with one scalar and one vector element for convenience:

$$\bar{u}^{s'}(p')\gamma_5\gamma^\mu u^s(p) \approx \begin{pmatrix}(\vec{p}'+\vec{p})\cdot\xi^{s'\dagger}\vec{\sigma}\xi^s\\ 2m\xi^{s'\dagger}\vec{\sigma}\xi^s\end{pmatrix}. \tag{3.55}$$

Expanding the second bilinear, we get

$$\begin{aligned}
&\bar{u}^{s'}(p')\sigma^{\mu\nu}u^s(p) = \frac{i}{2}u^{s'}(p')\left[\gamma^\mu,\,\gamma^\nu\right]u^s(p) = \\
&= \frac{i}{2}u^{s'}(p')\left(\begin{pmatrix}0 & \sigma^\mu\\ \bar{\sigma}^\mu & 0\end{pmatrix}\begin{pmatrix}0 & \sigma^\nu\\ \bar{\sigma}^\nu & 0\end{pmatrix} - \begin{pmatrix}0 & \sigma^\nu\\ \bar{\sigma}^\nu & 0\end{pmatrix}\begin{pmatrix}0 & \sigma^\mu\\ \bar{\sigma}^\mu & 0\end{pmatrix}\right)u^s(p) = \\
&= \frac{i}{2}u^{s'}(p')\left(\begin{pmatrix}\sigma^\mu\bar{\sigma}^\nu & 0\\ 0 & \bar{\sigma}^\nu\sigma^\mu\end{pmatrix} - \begin{pmatrix}\sigma^\nu\bar{\sigma}^\mu & 0\\ 0 & \bar{\sigma}^\mu\sigma^\nu\end{pmatrix}\right)u^s(p) = \\
&= \frac{i}{2}u^{s'}(p')\begin{pmatrix}\sigma^\mu\bar{\sigma}^\nu - \sigma^\nu\bar{\sigma}^\mu & 0\\ 0 & \bar{\sigma}^\nu\sigma^\mu - \bar{\sigma}^\mu\sigma^\nu\end{pmatrix}u^s(p).
\end{aligned} \tag{3.56}$$

Inserting the non-relativistic reduction of $u^s(p)$ and $\bar{u}^{s'}(p')$ while once again keeping only terms up to first order in $\vec{p}$, we get [48]

$$\begin{aligned}
&\bar{u}^{s'}(p')\sigma^{\mu\nu}u^s(p) \approx \\
&\approx \begin{pmatrix}0 & i(\vec{p}-\vec{p}')\mathbb{1} - (\vec{p}+\vec{p}')\times\xi^{s'\dagger}\vec{\sigma}\xi^s\\ -i(\vec{p}-\vec{p}')\mathbb{1} + (\vec{p}+\vec{p}')\times\xi^{s'\dagger}\vec{\sigma}\xi^s & 0\end{pmatrix}.
\end{aligned} \tag{3.57}$$

With the non-relativistic reduction of the bilinears at hand, we can form the two combinations that arise from scattering of a dark matter particle χ off a nucleus N.

They are, once again keeping only first order terms in momenta:

$$\begin{aligned}
&\bar{u}_\chi^{s'}(p')\gamma_5\gamma^\mu u_\chi^s(p)\bar{u}_N^{r'}(k')\gamma_5\gamma_\mu u_N^r(k) \approx \\
&\approx \begin{pmatrix} (\vec{p}\,' + \vec{p}) \cdot \xi^{s'\,\dagger}\vec{\sigma}\xi^s \\ 2m_\chi \xi^{s'\,\dagger}\vec{\sigma}\xi^s \end{pmatrix} \cdot \begin{pmatrix} (\vec{k}\,' + \vec{k}) \cdot \xi^{r'\,\dagger}\vec{\sigma}\xi^r \\ -2m_N \xi^{r'\,\dagger}\vec{\sigma}\xi^r \end{pmatrix} = \\
&= -4m_\chi m_N \xi^{s'\,\dagger}\vec{\sigma}\xi^s \xi^{r'\,\dagger}\vec{\sigma}\xi^r,
\end{aligned} \tag{3.58}$$

which in terms of the spin operators defined in equation (3.12) can be written

$$\bar{u}_\chi^{s'}(p')\gamma_5\gamma^\mu u_\chi^s(p)\bar{u}_N^{r'}(k')\gamma_5\gamma_\mu u_N^r(k) \approx -16 m_\chi m_N \vec{S}_\chi \cdot \vec{S}_N. \tag{3.59}$$

Here we recognise the operator $\mathcal{O}_4$ from Table 3.1. In a similar manner, excluding higher order momenta terms and inserting spin operators, the second relevant bilinear combination becomes (see e.g. [49])

$$\bar{u}_\chi^{s'}(p')\sigma^{\mu\nu} u_\chi^s(p)\bar{u}_N^{r'}(k')\sigma_{\mu\nu} u_N^r(k) \approx 16 m_\chi m_N \vec{S}_\chi \cdot \vec{S}_N, \tag{3.60}$$

where the operator $\mathcal{O}_4$ once again appears. This result, obviously only applicable to the specific framework of a solely spin dependent interaction theory, reveals that only two of the dark matter response functions $R_k^{\tau\tau'}$ (defined in equation (3.44)) are non-zero. Their definitions in terms of nucleons in the target are in general rather complicated, but are covered in good detail in literature [45]. The two that appear here are:

$$R_{\Sigma'}^{\tau\tau'} = R_{\Sigma''}^{\tau\tau'} = \frac{J_A\,(J_A+1)}{12} c_4^\tau c_4^{\tau'}, \tag{3.61}$$

where J_A denotes the nuclear spin of a target nucleus with mass number A. c_4^τ and $c_4^{\tau'}$ are the coefficients of the operator $\mathcal{O}_4$ in the amplitude in equation (3.38). They are in this case functions of the dark matter-nucleon couplings $\xi_{p,e}$, $\xi_{p,o}$, $\xi_{n,e}$, $\xi_{n,o}$ and the dark matter and target nucleus masses m_χ and m_A. Given a target nucleus with known nuclear response functions $W_k^{\tau,\tau'}$, that can be derived from single nucleons (see e.g. [45]), we can now construct a dark matter-nucleus cross section from nucleon level theory by combining our findings in this section with equations (3.35) and (3.38).

3.9 Dark matter-nucleus differential cross sections

The spin dependent differential cross section for dark matter χ and a target nucleus A scattering at recoil energy E_R can be written into the form [47]

$$\begin{aligned}
&\frac{d\sigma_{\mathrm{SD}}^A}{dE_R} = \\
&= \frac{16\mu_{\chi A}^2}{(2J_A+1)\,E_{\max}(v)} \left(\sqrt{S_{00}}(\xi_p+\xi_n) + \sqrt{S_{11}}(\xi_p-\xi_n)\right)^2 \Theta\left(E_{\max}(v) - E_R\right),
\end{aligned} \tag{3.62}$$

where we, as anticipated from the last section, see that both Lagrangian couplings and the particle masses are present, as well as the nuclear spin J_A of the target. The step function $\Theta\left(E_{\max}(v) - E_R\right)$ sets an upper limit for the recoil energy E_R

at the maxmimum recoil energy $E_{\max}(v)$, meaning that $0 < E_R < E_{\max}(v)$. For non-relativistic scattering, $E_{\max}(v)$ is given by

$$E_{\max}(v) = 2\frac{v^2\mu_{\chi A}^2}{m_A^2}. \tag{3.63}$$

From here on, the restriction $0 < E_R < E_{\max}(v)$ will be assumed to be implicit, and $\Theta\left(E_{\max}(v) - E_R\right)$ will thus be dropped from the differential cross section expressions.

Some further remarks on the differential cross section in equation (3.62) are needed in order to connect it to our earlier discussion. The Lagrangian couplings have been collected in the quantities ξ_p and ξ_n as

$$\xi_p = \frac{\xi_{p,e} + \xi_{p,o}}{2} \tag{3.64}$$

and

$$\xi_n = \frac{\xi_{n,e} + \xi_{n,o}}{2}. \tag{3.65}$$

The nuclear structure functions S_{00} and S_{11} are expressed in terms of the nuclear form factors $W_{\Sigma'}^{ij}$, $W_{\Sigma''}^{ij}$ as

$$S_{00} = W_{\Sigma'}^{00} + W_{\Sigma''}^{00} \tag{3.66}$$

and

$$S_{11} = W_{\Sigma'}^{11} + W_{\Sigma''}^{11}. \tag{3.67}$$

For a Majorana fermion, i.e. a fermion whose Lagrangian is invariant under the exchange $\psi_\chi \leftrightarrow \bar{\psi}_\chi$, the odd couplings are $\xi_{p,o} = \xi_{n,o} = 0$. The differential cross section in equation (3.62) then becomes

$$\begin{aligned}
&\frac{d\sigma_{\mathrm{SD,\,M}}^A}{dE_R} = \\
&= \frac{16\mu_{\chi A}^2}{(2J_A+1)\,E_{\max}(v)}\left(\sqrt{S_{00}}(\xi_p^M + \xi_n^M) + \sqrt{S_{11}}(\xi_p^M - \xi_n^M)\right)^2 = \\
&= \frac{16\mu_{\chi A}^2}{(2J_A+1)\,E_{\max}(v)}\left(\sqrt{S_{00}}\lambda_{00}^M + \sqrt{S_{11}}\lambda_{11}^M\right)^2,
\end{aligned} \tag{3.68}$$

where $\xi_N^M \equiv \frac{\xi_{N,e}}{2}$ and thus

$$\lambda_{00}^M \equiv \frac{\xi_{p,e} + \xi_{n,e}}{2} \tag{3.69}$$

and

$$\lambda_{11}^M \equiv \frac{\xi_{p,e} - \xi_{n,e}}{2}. \tag{3.70}$$

For a Dirac dark matter particle, the differential cross section would be the same, but with

$$\xi_N^M \to \xi_N^D \equiv \frac{\xi_{N,e} + \xi_{N,o}}{2}. \tag{3.71}$$

For a Dirac antiparticle, the new coupling would instead be

$$\xi_N^M \to \xi_N^{\bar{D}} \equiv \frac{\xi_{N,e} - \xi_{N,o}}{2}, \tag{3.72}$$

where the difference in sign of the odd couplings $\xi_{N,o}$ is due to the conjugation of the Lagrangian when changing between a particle field ψ_χ and antiparticle field $\bar{\psi}_\chi$. In the standard freeze-out scenario, the contribution from particle and antiparticle dark matter would be the same [50]. This means that the Dirac differential cross section should be split in one part for particles and one part for antiparticles, giving

$$\begin{aligned}\frac{d\sigma^A_{\mathrm{SD,\,D}}}{dE_R} &= \frac{1}{2}\left[\frac{d\sigma^A_{\mathrm{SD,\,particle}}}{dE_R} + \frac{d\sigma^A_{\mathrm{SD,\,antiparticle}}}{dE_R}\right] = \\ &= \frac{16\mu^2_{\chi A}}{(2J_A+1)\,E_{\max}(v)}\frac{1}{2}\Big[\left(\sqrt{S_{00}}(\xi^D_p+\xi^D_n)+\sqrt{S_{11}}(\xi^D_p-\xi^D_n)\right)^2 + \\ &+ \left(\sqrt{S_{00}}(\xi^{\bar{D}}_p+\xi^{\bar{D}}_n)+\sqrt{S_{11}}(\xi^{\bar{D}}_p-\xi^{\bar{D}}_n)\right)^2\Big] = \\ &= \frac{16\mu^2_{\chi A}}{(2J_A+1)\,E_{\max}(v)}\frac{1}{2}\Big[S_{00}\left((\xi^D_p+\xi^D_n)^2+(\xi^{\bar{D}}_p+\xi^{\bar{D}}_n)^2\right) + \\ &+ 2\sqrt{S_{00}S_{11}}\left(\xi^{D\,2}_p-\xi^{D\,2}_n+\xi^{\bar{D}\,2}_p-\xi^{\bar{D}\,2}_n\right) + \\ &+ S_{11}\left((\xi^D_p-\xi^D_n)^2+(\xi^{\bar{D}}_p-\xi^{\bar{D}}_n)^2\right)\Big].\end{aligned} \tag{3.73}$$

By defining coefficients of the nuclear structure form factors, this differential cross section can be cast into a more perspicuous form. As can be seen in equation (3.73), they can be conveniently chosen as

$$\lambda^2_{00} = \frac{1}{2}\left[(\xi^D_p+\xi^D_n)^2+(\xi^{\bar{D}}_p+\xi^{\bar{D}}_n)^2\right], \tag{3.74}$$

$$\lambda^2_{11} = \frac{1}{2}\left[(\xi^D_p-\xi^D_n)^2+(\xi^{\bar{D}}_p-\xi^{\bar{D}}_n)^2\right], \tag{3.75}$$

$$f = \frac{\xi^{D\,2}_p-\xi^{D\,2}_n+\xi^{\bar{D}\,2}_p-\xi^{\bar{D}\,2}_n}{2\lambda_{00}\lambda_{11}}, \tag{3.76}$$

and the Dirac differential cross section can now be expressed as

$$\begin{aligned}\frac{d\sigma^A_{\mathrm{SD,\,D}}}{dE_R} &= \\ &= \frac{16\mu^2_{\chi A}}{(2J_A+1)\,E_{\max}(v)}\left[S_{00}\lambda^2_{00}+2\sqrt{S_{00}S_{11}}\lambda_{00}\lambda_{11}f+S_{11}\lambda^2_{11}\right] = \\ &= \frac{16\mu^2_{\chi A}}{(2J_A+1)\,E_{\max}(v)}\Big[\left(\sqrt{S_{00}}\lambda_{00}+\sqrt{S_{11}}\lambda_{11}\right)^2+2\sqrt{S_{00}S_{11}}\lambda_{00}\lambda_{11}(f-1)\Big].\end{aligned} \tag{3.77}$$

Rewriting the differential cross section in this way makes it apparent that the only particle model dependency comes from the three free parameters f, λ_{00} and λ_{11}, the rest of the parameters are properties of the target nucleus. An important observation can now be made for two values of f, more precisely $f=-1$ and $f=1$.

For these values of f, the Dirac differential cross section in equation (3.77) reduces to the Majorana differential cross section in equation (3.68) under the identification $\lambda^M_{00}=\lambda_{00}$ and $\lambda^M_{11}=\pm\lambda_{11}$. This feature of the differential cross section is an

important attribute to the test procedure for discriminating between Majorana and Dirac dark matter, and will be discussed in more detail in the next section when we outline the discrimination test.

3.10 Differences between spin dependent and spin independent cross sections

Having seen how the differential cross section for spin dependent interactions is calculated, we make a quick detour to investigate how it compares to the differential cross section for spin independent interactions. This reveals some interesting differences in the particle physics input in cross section calculations. This section aims to demonstrate these differences. The main difference between the two studies is the choice of Lagrangian to consider. Kavanagh et al. uses the first two (spin independent) terms in equation (3.45), and in this thesis we use the second two (spin dependent) terms instead. The differences are presented in order to expose the fundamental changes that has to be done when moving between spin dependent and spin independent interaction theory. Even though these differences are not of particular interest for this study, they are interesting when for instance comparing measured cross sections to experimental thresholds.

3.10.1 Change in free parameters

In the spin independent interaction theory, the differential cross section scales with the number of protons N_p and neutrons N_n in the target as [3]

$$\frac{d\sigma_{SI}}{dE_R} \propto (\lambda_p N_p + \lambda_n N_n)^2 + 2\lambda_p \lambda_n (f-1) N_p N_n, \tag{3.78}$$

where the three free parameters λ_p, λ_n and f depend on the underlying particle physics interaction model. It can be seen that all the particle physics, up to a global scaling, can be encoded into the two parameters $\{f, \lambda_p/\lambda_n\}$ [3]. When considering the spin dependent part of the theory instead, we have seen that the differential cross section is given as a function of the nuclear form factor functions S_{00} and S_{11}. However, the scaling with these quantities turns out to be similar to the one in equation (3.78), more specifically

$$\frac{d\sigma_{SD}}{dE_R} \propto \left(\lambda_{00}\sqrt{S_{00}} + \lambda_{11}\sqrt{S_{11}}\right)^2 + 2\lambda_{00}\lambda_{11}(f-1)\sqrt{S_{00}S_{11}}, \tag{3.79}$$

and we observe that the free parameters in this case are λ_{00}, λ_{11} and f, meaning that the used parameter space for the spin dependent study presented here will be given by $\{f,\ \lambda_{11}/\lambda_{00}\}$. This will be seen more in detail in chapter 4.

3.10.2 Change in nucleus and nucleon cross section

This section gives a brief summary of some differences between the proton cross sections of spin independent and spin dependent theory, which is used when comparing

and constructing cross section thresholds for dark matter-nucleus interactions. As per [47], the cross section in the zero momentum transfer limit for the spin independent theory is

$$\sigma_{\mathrm{SI}}^{A} = \frac{4\mu_{\chi A}^{2}}{\pi} \left(\lambda_p N_p + \lambda_n N_n\right)^2 , \tag{3.80}$$

and for spin dependent theory it is

$$\sigma_{\mathrm{SD}}^{A} = \frac{16\mu_{\chi A}^{2}}{\pi} \frac{J_A + 1}{J_A} \left(\xi_p S_p + \xi_n S_n\right)^2 , \tag{3.81}$$

where S_p and S_n are functions that can be absorbed into our earlier defined S_{00} and S_{11}. In fact, these nucleus cross sections can be decomposed in terms of the proton-dark matter cross section $\sigma_{\mathrm{SI/SD}}^{p}$, which for isospin-violating dark matter turns out to be the relevant quantity to compare when studying potential direct detection signals [51]. In the spin independent theory, the cross section in equation (3.80) appears as

$$\sigma_{\mathrm{SI}}^{A} = \sigma_{\mathrm{SI}}^{p} \left(N_p + \frac{\lambda_n}{\lambda_p} N_n\right)^2 , \tag{3.82}$$

where the spin independent proton cross section is defined as [51]

$$\sigma_{\mathrm{SI}}^{p} \equiv \frac{4\mu_{\chi p}^{2}}{\pi} \lambda_p^2 . \tag{3.83}$$

The value of σ_{SI}^{p} can then be used to normalise the theory with respect to experimental constraints of the values of the cross section. In the spin dependent case, the proton-dark matter cross section is instead [51]

$$\sigma_{\mathrm{SD}}^{p} \equiv \frac{3\mu_{\chi p}^{2}}{\pi} \xi_p^2 , \tag{3.84}$$

which gives the nucleus-dark matter cross section at rest

$$\begin{aligned} &\sigma_{\mathrm{SD}}^{A} = \\ &= \frac{16}{3(2J_A + 1)} \frac{\mu_{\chi A}^{2}}{\mu_{\chi p}^{2}} \sigma_{\mathrm{SD}}^{p} \left[\left(\sqrt{S_{00}} + \sqrt{S_{11}}\right) + \left(\sqrt{S_{00}} - \sqrt{S_{11}}\right) \frac{\xi_n}{\xi_p}\right]^2 . \end{aligned} \tag{3.85}$$

4
Methods

4.1 Description of the test

A test method for rejecting Majorana in favour of Dirac dark matter for spin-independent interactions was published by Bradley J. Kavanagh et al. in 2017 [3]. This study constitutes the basis for the test presented in this thesis, which instead will be developed in the spin dependent interaction theory introduced in the last chapter. As described in equation (3.77), in the case of Dirac dark matter, the spin dependent differential cross section for dark matter-nucleus scattering includes a term which is missing for Majorana dark matter. I will show that the extra term in the cross section for Dirac dark matter allows for rejection of the Majorana hypothesis in favour of the Dirac hypothesis. The most straightforward way to describe the proposed test is as follows. One assumes Majorana nature, measures the cross section for a set of different targets and then compares theory with observations to see if the extra term in the cross section is present or not. This description leaves out a lot of important subtleties, more details are presented below.

4.1.1 Detailed test procedure

The difference in Majorana and Dirac dark matter differential cross section should, in theory, make it possible to distinguish between the two, given that measurements of scattering cross sections are made. Assuming Majorana dark matter, and that two targets X and Y have given a scattering signal due to dark matter nucleus interactions, the measured cross sections would be (as per integration of equation (3.77)):

$$\sigma^X_{\mathrm{SD,\,M}} = \frac{16\mu^2_{\chi X}}{2J_X+1}\left(\sqrt{S^X_{00}}\lambda^M_{00} + \sqrt{S^X_{11}}\lambda^M_{11}\right)^2, \tag{4.1}$$

$$\sigma^Y_{\mathrm{SD,\,M}} = \frac{16\mu^2_{\chi Y}}{2J_Y+1}\left(\sqrt{S^Y_{00}}\lambda^M_{00} + \sqrt{S^Y_{11}}\lambda^M_{11}\right)^2. \tag{4.2}$$

These two equations can be rewritten as

$$\frac{\sigma^X_{\mathrm{SD,\,M}}(2J_X+1)}{16\mu^2_{\chi X}} = \left(\sqrt{S^X_{00}}\lambda^M_{00} + \sqrt{S^X_{11}}\lambda^M_{11}\right)^2, \tag{4.3}$$

$$\frac{\sigma^Y_{\mathrm{SD,\,M}}(2J_Y+1)}{16\mu^2_{\chi Y}} = \left(\sqrt{S^Y_{00}}\lambda^M_{00} + \sqrt{S^Y_{11}}\lambda^M_{11}\right)^2. \tag{4.4}$$

Given an experimental measurement of the cross sections and the relevant target properties J_A and $\mu_{\chi A}$, the left hand side of each of these two equations is known. Since the target nucleus properties are assumed to be determined, the values of S_{00}^X, S_{11}^X, S_{00}^Y and S_{11}^Y are known as well. Effectively, the two equations (4.3) and (4.4) then describe two parallel lines *each* in the $\{\lambda_{00}^M, \lambda_{11}^M\}$ parameter space. The slope of each pair of lines is $k_X = \sqrt{S_{00}^X/S_{11}^X}$ and $k_Y = \sqrt{S_{00}^Y/S_{11}^Y}$ respectively. Thereby, for $k_X \neq k_Y$, there will always be four different intersection points between the four lines. In these four intersection points, the values of $\{\lambda_{00}^M, \lambda_{11}^M\}$ will be consistent with both experiment X an Y. Note that changing the signs, i.e. letting $\{\lambda_{00}^M, \lambda_{11}^M\} \to \{-\lambda_{00}^M, -\lambda_{11}^M\}$, connects the four solutions with each other in such a way that actually only two of them are different. This means that there in practice only will be two intersection points of interest. This is shown in Figure 4.1, where each experimental measurement of a cross section corresponds to two parallel lines.

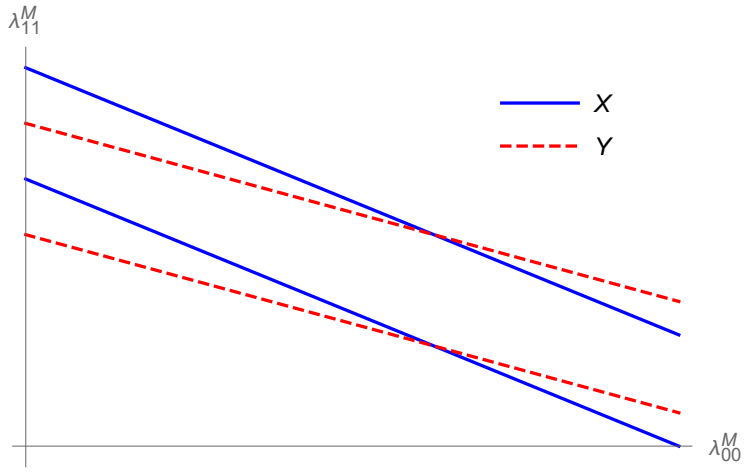

Figure 4.1: The four lines in $\{\lambda_{00}^M, \lambda_{11}^M\}$ parameter space due to the two measured cross sections for experiment X and Y. The two cross sections are consistent with each other at the intersection points of the lines, where the values of $\{\lambda_{00}^M, \lambda_{11}^M\}$ agree.

In conclusion, two measurements of signals from dark matter scattering off different targets can always be described by a rescaled Majorana model. However, if one were to add a third experiment Z and measure the cross section $\sigma_{\mathrm{SD,M}}^Z$, a new set of parallel lines would be introduced, allowing for two different outcomes:

1. One or both of the new lines passes through one of the two intersection points that are compatible with experiment X and Y. This means that up to a sign difference, the values of $\{\lambda_{00}^M, \lambda_{11}^M\}$ would have been determined. In this case all three experiments would then be consistent with the Majorana particle nature, and we would thus not be able to tell it apart from Dirac. One such outcome is depicted to the left in Figure 4.2.
2. None of the new lines passes through the earlier intersection points. This would imply that the three measurement are inconsistent. The assumption of Majorana dark matter would then be wrong, meaning that it must be of Dirac nature. One such outcome is depicted to the right in Figure 4.2.

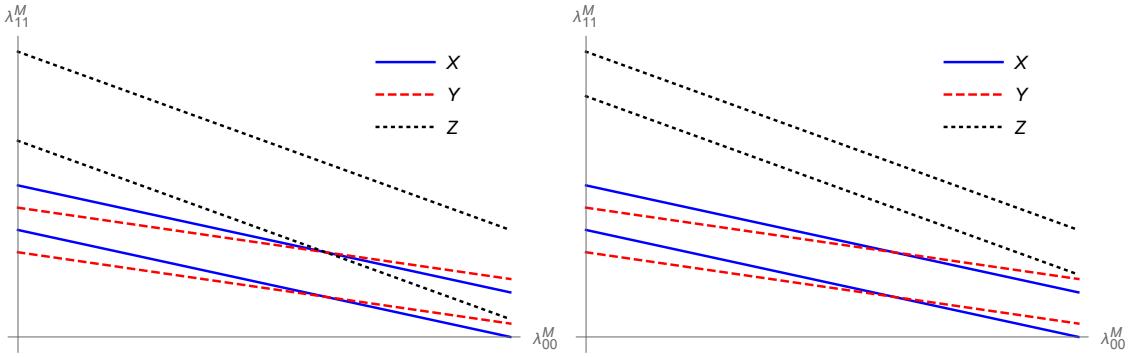

Figure 4.2: Two examples of possible outcomes after adding a third experiment Z to the test procedure. To the left all three experiments agree on a set of values $\{\lambda_{00}^M, \lambda_{11}^M\}$, making discrimination impossible. To the right, there is no point at which all three experiments agree on a set of values, and discrimination is thereby possible.

An important attribute of the test has now been revealed; within the given framework for fermionic dark matter, it can only confirm the nature of Dirac dark matter. It will never be able to verify the Majorana nature, as all measurements will always be consistent with each other in this case. A more direct explanation of this phenomena can be seen by comparing equations (3.68) and (3.73). The Dirac differential cross section can always be reduced to a Majorana-like form, but not the other way around. This asymmetry of the test can also be seen in a third way, by looking at the Lagrangian of the theory in equation (3.46). The even terms, corresponding to axial vector interactions, are present for both particle nature descriptions, but only Dirac nature has odd terms that correspond to tensor interactions. The Majorana Lagrangian is thus a special case of the Dirac Lagrangian, leading us to the same conclusion regarding the test as before.

4.1.2 Properties of the test

As concluded in the last section, in order to discriminate between Dirac or Majorana dark matter, the detected scattering events must be from a Dirac particle. We have seen that the nucleon Lagrangian couplings can be rewritten into $\{\lambda_{00}^M, \lambda_{11}^M\}$ for Majorana dark matter and $\{\lambda_{00}, \lambda_{11}, f\}$ for Dirac dark matter. If the measurements are due to a Dirac dark matter particle, the test will boil down to comparing the three measured cross sections under the two different particle nature assumptions. For the three different experiments, this is described by the following system of equations:

$$\sigma_{\mathrm{SD,\,M}}^A = \sigma_{\mathrm{SD,\,D}}^A, \tag{4.5}$$

where the targets A runs over $A = X, Y, Z$. If we can find values of $\lambda_{00}^M, \lambda_{11}^M$ that makes this system inconsistent, we would successfully have excluded Majorana dark matter and thereby confirmed the particle nature to be described by Dirac theory. At this point, we can observe that several parameters that have influence on the cross section, such as the nucleus spin J_A and reduced mass $\mu_{\chi A}$, does not affect

if the system is consistent or not. This is because of the common factors of the differential cross sections, as can be seen in equations (3.68) and (3.73). Another, perhaps more astonishing, observation is that the comparison of the cross section works equally good under a global rescaling of the couplings, so the actual value of the cross sections are not of relevance. Only eventual differences in the actual values of the cross sections matters in this case, but the accuracy with which the cross section can be measured depend on the coupling constant values. For applications of the test, a more interesting question is the opposite: what parameters are the ones that does matter for the comparison? As described earlier in this test description (see e.g. equation (4.3) and the following discussion), the relevant parameters are actually the square root of the nuclear structure functions

$$k_A = \sqrt{\frac{S_{00}^A}{S_{11}^A}}, \tag{4.6}$$

for the different targets. The test is highly sensitive to changes in this quantity, and as discussed above, it relies on the targets having different values for k_A.

4.1.3 Choice of targets

In the spin independent test [3], the target property of importance is the number of protons divided by the number of neutrons N_p/N_n rather than the quantity $\sqrt{S_{00}/S_{11}}$. This means that the choice of targets in the spin independent case is made with respect to proton-to-neutron ratios, while in the spin dependent case the choice will be based on values of $\sqrt{S_{00}/S_{11}}$ instead. These values for some standard dark matter direct detection targets [45], have been gathered in Table 4.1.

It would be convenient if the targets with maximal differences in the two quantities would overlap, so that the same experiments could be used to carry out both the spin dependent and spin independent test. Unfortunately, this does not seem to be the case for the standard dark matter direct detection targets studied here. For instance, silicon and argon make great targets when studying potential spin independent signals due to their big difference in proton-to-neutron ratio, as can be seen in Table 4.1. It is also apparent from there that both silicon and argon are useless for studying spin dependent theory, as their nuclear spin is zero. The optimal choice of targets to study is thus different in the two cases. In the spin dependent case considered here, the target setup constructed from Table 4.1 that gives the best spread in $\sqrt{S_{00}/S_{11}}$ is $\{^{127}\text{I}, ^{23}\text{Na}, ^{19}\text{F}\}$. The discrimination procedure was thus based on this set of targets, and the results are presented in chapter 5.

However, in the case that one wants to study both spin independent and spin dependent interactions at once, it can also be seen from Table 4.1 that choosing targets that have quantities suitable for both should be possible, but some compromises would have to be made. For instance, considering experimental data from the three experiments ^{131}Xe, ^{127}I and ^{73}Ge, one should in theory have values of N_p/N_n and $\sqrt{S_{00}/S_{11}}$ that are different enough between the targets to be able to use them simultaneously for both purposes, but since xenon and germanium have similar values for $\sqrt{S_{00}/S_{11}}$, the area in parameter space where discrimination is possible might

turn out to be small. A test based on this setup is presented in chapter 5 as well.

Nucleus	N_p/N_n	$\sqrt{S_{00}/S_{11}}$
Silicon (^{28}Si)	1.0	0
Argon (^{40}Ar)	0.82	0
Germanium (^{73}Ge)	0.78	1.03
Xenon (^{131}Xe)	0.70	1.05
Iodine (^{127}I)	0.72	1.66
Sodium (^{23}Na)	0.92	1.17
Fluorine (^{19}F)	0.9	0.96

Table 4.1: A summary of potential dark matter experiment targets and their values of the quantities N_p/N_n and $\sqrt{S_{00}/S_{11}}$. The values for S_{00} and S_{11} were obtained using `dmformfactor`, see section 4.2.

As this thesis only looks at one particular isotope of all the target elements in Table 4.1, the atomic number is from here on dropped for simplicity. For instance; ^{28}Si will from now on be written as Si, ^{40}Ar as Ar etc.

4.1.4 Restriction on parameters for which the tests works

As observed, the quantity that decides what target candidates to use is $\sqrt{S_{00}/S_{11}}$. A crucial condition for being able to discriminate between Dirac and Majorana is then that all targets have different values for this quantity. However, it turns out that standard stable nuclear targets have very similar values, as seen in Table 4.1. As a result of this, the values of $\sigma^A_{\mathrm{SD,\,M}}$ and $\sigma^A_{\mathrm{SD,\,D}}$ will be so close that their difference will fall within experimental and statistical uncertainties [3]. This seems to make the test impossible to carry out in practice, but there are certain combinations of parameters where the difference between $\sigma^A_{\mathrm{SD,\,M}}$ and $\sigma^A_{\mathrm{SD,\,D}}$ is bigger. This phenomena appears when the parameters λ^M_{00}, λ^M_{11} and f are such that there is a cancellation in the first term of the Dirac cross section in one of the targets. As can be seen from e.g. equation (3.77), such cancellations takes place when $\lambda^M_{11}/\lambda^M_{00} = -\sqrt{S_{00}/S_{11}}$, where λ^M_{00} and λ^M_{11} are decided from measurements. When this happens for a target A, it gets no contribution from the first term in the cross section. As we know, the Majorana cross section only has the first term, so effectively we get

$$\sigma^A_{\mathrm{SD,\,M}} = 0 \tag{4.7}$$

and

$$\sigma^A_{\mathrm{SD,\,D}} \propto 2\lambda^M_{00}\lambda^M_{11}(f-1)\sqrt{S_{00}S_{11}} = -2\lambda^{M\,2}_{00}(f-1)S_{00}, \tag{4.8}$$

where we have used that $\lambda^M_{11} = -\lambda^M_{00}\sqrt{S_{00}/S_{11}}$.The problem to make the difference between $\sigma^A_{\mathrm{SD,\,M}}$ and $\sigma^A_{\mathrm{SD,\,D}}$ as large as possible has thus been reduced to making the value of $\sigma^A_{\mathrm{SD,\,D}}$ as large as possible. From equation (4.8), we see that this happens when f is close to -1. In conclusion, the test is possible to carry out if:

- $\lambda_{11}/\lambda_{00} \approx \sqrt{\frac{S_{00}}{S_{11}}}$,
- $f \approx -1$,

where we have used that $-\lambda_{11}^M/\lambda_{00}^M = \lambda_{11}/\lambda_{00}$ for $f \approx -1$, as seen from equation (3.77). Note that this constraint only needs to be fulfilled for one of the targets. In fact, if this cancellation happens for two targets, the test will fail, as only one cross section would then be measured. This is also a problem that arises if two of the targets have too similar values of $\sqrt{S_{00}/S_{11}}$, meaning that the cancellation in one of them will bring a partial cancellation in the other one as well. This effect is shown in a comparison in the results, see Figure 5.3.

4.1.5 Other limitations of the test

In the discussion of the last section we have four fundamental even/odd dark matter-nucleon couplings (ξ_p^D, ξ_n^D, $\xi_p^{\bar{D}}$, $\xi_n^{\bar{D}}$), where only ξ_p^D and ξ_n^D appear for Majorana dark matter. We have also seen that these couplings can actually be written in terms of three free parameters for each particle nature description, $\{\lambda_{00}^M, \lambda_{11}^M, f\}$ for Majorana and $\{\lambda_{00}, \lambda_{11}, f\}$ for Dirac. This means that in the end the differential cross section only depends on these three parameters, and it follows that there is no way to, by considering direct detection experiments only, break the degeneracy between the four fundamental dark matter-nucleon couplings by using the presented test.

The overlap between the two differential cross sections in equations (3.68) and (3.77) constitutes the foundation of the discrimination test, but for coupling values that gives exactly $f = \pm 1$, the test would end up failing to work, as both Dirac and Majorana dark matter then would give the same differential cross section. Regions in parameter space where this is the case will then be inconclusive already from a theoretical perspective. All cases where the Majorana and Dirac direct detection cross section has the same signal will make the text inconclusive. In practice, this happens when:

- The Dirac fermion only interacts either via axial vector or tensor interactions, but only one of them. This corresponds to the spin dependent Lagrangian only having one of the two terms considered here.
- The dark matter couples only to protons or neutrons, but not both. This would imply that $\lambda_{00}^M = \lambda_{11}^M$ and $\lambda_{00} = \lambda_{11}$ in the two models, taking away the possibility of the right combinations of couplings for discrimination.
- The particle or antiparticle cross section of the Dirac signal is zero for all nucleus *or* the density of dark matter particles/antiparticles is very different from each other (note that these densities here are assumed to be equal).
- The value of the couplings to protons over the coupling to neutrons is the same for particle and antiparticle dark matter, i.e. $\frac{\xi_p^D}{\xi_n^D} = \frac{\xi_p^{\bar{D}}}{\xi_n^{\bar{D}}}$.

4.1.6 Application of the test to measurements

In practice, the test would need the experimental measurement of two cross sections $\sigma_{\mathrm{SD,\,M}}^X$ and $\sigma_{\mathrm{SD,\,M}}^Y$ to start with. From our earlier discussion, we know that this would give two sets of values for $\{\lambda_{00}^M, \lambda_{11}^M\}$. As the test assumes Majorana dark matter, these values of $\{\lambda_{00}^M, \lambda_{11}^M\}$ can be used to calculate the cross section $\sigma_{\mathrm{SD,\,M}}^Z$ that would

be expected from the third measurement, based on the cross section values of the first two. Also following the earlier discussion, the signal is assumed to be due to a Dirac dark matter particle which gives a cross section $\sigma^Z_{\mathrm{SD,\,D}}$, as a Majorana dark matter particle would not be identified by the test. The expected cross section $\sigma^Z_{\mathrm{SD,\,D}}$ can then be compared to the measured one with a measure δ defined as [3]

$$\delta = \frac{\left(\sigma^Z_{\mathrm{SD,\,D}} - \sigma^Z_{\mathrm{SD,\,M}}\right)^2}{\left(\sigma^Z_{\mathrm{SD,\,D}}\right)^2}. \tag{4.9}$$

Small values of this quantity means that the Majorana and Dirac description of the cross section have a big overlap, implying that the experimental setup considered is badly suited for the test. On the other hand, large values of δ suggests that the discrimination between Dirac and Majorana should be possible for the considered experimental setup. At this point, it becomes apparent that having similar $\sqrt{S_{00}/S_{11}}$ for two of the targets will make the test less conclusive. If the cancellation of the first term in the cross takes place for one of these two targets, it will approximately do so for the other one as well, giving a low cross section signal to study. In practice, it is thus of interest to choose targets such that:

- Target Z has a cancellation in the first term of the cross section, i.e. $\lambda_{11}/\lambda_{00} \approx \sqrt{S_{00}/S_{11}}$.
- The three targets have values of $\sqrt{S_{00}/S_{11}}$ that are well separated from each other.

The original test for the spin independent case came published together with Mathematica code for the plotting of δ as function of the spin independent couplings λ_p and λ_n [3]. This code was modified in order for it to be usable in the spin dependent case, i.e. to plot δ as a function of λ_{00} and λ_{11}. To illustrate the effect on the value of δ that comes from having different value of $\sqrt{S_{00}/S_{11}}$ for all targets, an experimental setup of {I, Na, F}, with $\sqrt{S_{00}/S_{11}} = \{1.66,\ 1.17,\ 0.96\}$ (as seen in Table 4.1), was studied and compared to another setup. This second setup was {I, Fake, F}, with $\sqrt{S_{00}/S_{11}} = \{1.66,\ 1/3,\ 0.96\}$, where Fake is a mock-target with the same properties as Na apart from the value of $\sqrt{S_{00}/S_{11}}$. A comparison of the δ_I-values for these setups is presented in Figure 5.1.

The value of δ_I for an experiment containing {I, Xe, Ge} was calculated, where Xe was included due to it being an important experimental target already implemented in direct detection searches [52], as well as having a suitable value of $\sqrt{S_{00}/S_{11}} = 1.05$. The resulting contour plot of δ_I is shown in Figure 5.2, together with the δ_I-value for {I, Na, F} for comparison. The experimental target setup {I, Xe, Ge} is also interesting because all of the targets have a non-zero value of both N_p/N_n and $\sqrt{S_{00}/S_{11}}$, making it a potential candidate setup to study both spin independent and spin dependent interactions.

4.2 Numerical tool for form factor calculations

As we have seen through this thesis, the spin dependent interaction between spin 1/2 dark matter particles and target nuclei depend on the form factor functions S_{00} and S_{11}, related to $W_k^{\tau\tau'}$ as described in equations (3.66) and (3.67). They describes the transition from nucleons to the target nucleus. These form factors can be found from experimental data input, in a way to form closed analytic expressions for the nucleus theory, given a nucleon theory input. These calculations were done in a open source Mathematica code called `dmformfactor` [45]. This code gives, with nucleus data as input, the nucleus form factors $W_k^{\tau\tau'}$. This is done by assuming a standard shell-model for the nucleons in the nucleus and expanding the nucleon wave functions in a harmonic oscillator basis, which leads to Slater-determinant expressions for $W_k^{\tau\tau'}$ in terms of nucleon spins. These calculations are explained in detail in [45]. One of the subroutines in `dmformfactor` directly returns the value of S_{00} and S_{11}. Using this function, expressions for S_{00} and S_{11} were obtained for Xe and Ge, two of the five targets proposed for the spin independent test in [3]. They are the only ones with nuclear spin out of the suggested targets for the spin independent study, and are thus included due to the overlap between their usability in both tests. In addition, the targets I, Na and F were added to this study, and their values of S_{00} and S_{11} where also calculated with `dmformfactor`. A list of all values for $\sqrt{S_{00}/S_{11}}$ studied here was given in Table 4.1.

4.3 Statistical procedure and discrimination

This section gives the foundation for the statistical procedure employed in [3], but other approaches, such as Bayesian statistics, could in principle also be used. This thesis does not include any statistical treatment of the test, but this section is included for completeness and as a starting point for eventual future use of the results presented here.

In the treatment of the particle physics in the test, we have seen that the set of parameter points in the spin dependent theory can actually be described entirely by the three free parameters λ_{00}, λ_{11} and f for a given dark matter mass m_χ. We have also seen that the relevant parameter space is actually given by the parameter point $\{\lambda_{11}/\lambda_{00},\, f\}$. At each such parameter point, a set of mock direct detection signals, i.e. a number of made up detector events, can be generated in the studied experimental ensemble. The maximum likelihood of obtaining the data can then be calculated under the two different hypothesis of Majorana and Dirac particle nature. As per the discussion above, this gives us the following structure of the two hypotheses, denoted $\mathbf{H}_M$ and $\mathbf{H}_D$ respectively:

- $\mathbf{H}_M$: Majorana dark matter, parameters $\mathbf{\Theta} = \{m_\chi,\, \lambda_{00},\, \lambda_{11},\, f = \pm 1\}$,
- $\mathbf{H}_D$: Dirac dark matter, parameters $\mathbf{\Theta} = \{m_\chi,\, \lambda_{00},\, \lambda_{11},\, f \in [-1,\, 1]\}$.

The likelihood used by Kavanagh et. al is a background-free extended likelihood. For experiment k, the likelihood considered is

$$\mathcal{L}_k(\Theta) = \frac{e^{-N_e(\Theta)}}{N_o!} \left(N_e(\Theta)\right)^{N_o} \Pi_{i=1}^{N_o} P(E_R^{(i)}|\Theta), \tag{4.10}$$

where N_o is the number of observed events in experiment k, observed at recoil energies $E_R^{(1)}, \ldots, E_R^{(N_o)}$. For a underlying set of parameters, given by $\mathbf{\Theta}$, N_e denotes the number of expected events in experiment k. Finally, $P(E_R^{(i)}|\Theta)$ is the probability of an event at energy E_R to be measured. From this experiment-likelihood, the full likelihood for all included experiments is given by

$$\mathcal{L}(\Theta) = \Pi_k^{N_{\text{exper.}}} \mathcal{L}_k(\Theta), \tag{4.11}$$

with $N_{\text{exper.}}$ denoting the number of experiments considered. Under each of the two hypotheses $\mathbf{H}_M$ and $\mathbf{H}_D$, the maximum likelihood, i.e. the largest possible value of $\mathcal{L}(\Theta)$, can be obtained by sampling the parameters $\{\lambda_{11}/\lambda_{00},\, f\}$ on a grid around the point where the cancellation in the first term in the cross section takes place. We denote these maxima as $\hat{\mathcal{L}}_M$ and $\hat{\mathcal{L}}_D$ respectively. The likelihood described in equation (4.11) turns out to be possibly multimodal, making obtaining $\hat{\mathcal{L}}_M$ and $\hat{\mathcal{L}}_D$ complicated. A detailed explanation of how this problem is solved is discussed in Appendix A of the spin independent test [3]. When one has found $\hat{\mathcal{L}}_M$ and $\hat{\mathcal{L}}_D$, a test statistic q, defined as

$$q = -2(\log\hat{\mathcal{L}}_M - \log\hat{\mathcal{L}}_D), \tag{4.12}$$

can be formed to compare the two maximum likelihoods. This test statistic is, under the Majorana hypothesis, asymptotically half chi-squared distributed with one degree of freedom [3, 53]. The one degree of freedom is due to the extra non-restrained parameter f that appears in $\mathbf{H}_D$ and not in $\mathbf{H}_M$ [3]. From the q-value, one can obtain a corresponding p-value, i.e. the separation of the probability distribution for the Majorana and Dirac hypotheses, and from there obtain the significance at which the Majorana hypothesis $\mathbf{H}_M$ can be rejected in favour of the Dirac hypothesis $\mathbf{H}_D$.

In order to carry out the statistical analysis in practice, one would have to simulate mock data for the observed number of events N_o under the two different hypotheses (or use future experimental data, if dark matter signals are found). The number of events is related to the different cross sections of the two theories by integration of equation (2.8). For a given number of observed events, one would then be able conclude a significance at which theoretical discrimination is possible, as done by Kavanagh et al. [3].

5
Results

The main result found in this study is the effect that the quantity $\sqrt{S_{00}/S_{11}}$ has on the discrimination probability. We have seen that larger difference in this quantity between the targets makes identifying Dirac particles easier, and we will now see how this quantity would effect discrimination for experiments consisting of three standard dark matter direct detection targets. As discussed in chapter 4, and therein defined as a function of the Dirac/Majorana cross sections σ^D and σ^M, we have calculated

$$\delta = \frac{\left(\sigma^D - \sigma^M\right)^2}{\left(\sigma^D\right)^2}, \tag{5.1}$$

for one of the three targets in each experimental setup. The region in $\{f,\ \lambda_{11}/\lambda_{00}\}$ parameter space where discrimination between Dirac and Majorana particles is most likely then reveals itself as the regions where δ takes large values. As earlier noted, the test compares ratios of the cross sections, meaning that their magnitude does not affect the tests outcome in theory. However, if the cross sections are too small, there will not be enough events to calculate their value in the first place, meaning that there will be no data to apply the test to.

In order to demonstrate the importance of having different values of $\sqrt{S_{00}/S_{11}}$ for the targets, a comparison between the setups {I, Na, F} and {I, Fake, F} is made for δ_I. Fake is a non-existing target nucleus with the same properties as sodium (Na), apart from having $\sqrt{S_{00}/S_{11}} = 1/3$. As per Table 4.1, iodine (I) has $\sqrt{S_{00}/S_{11}} = 1.66$ and sodium has $\sqrt{S_{00}/S_{11}} = 1.17$. This implies that the target setup {I, Fake, F} will have a larger difference of $\sqrt{S_{00}/S_{11}}$ between the targets than {I, Na, F}. This comparison of δ_I for the two setups can be seen in Figure 5.1.

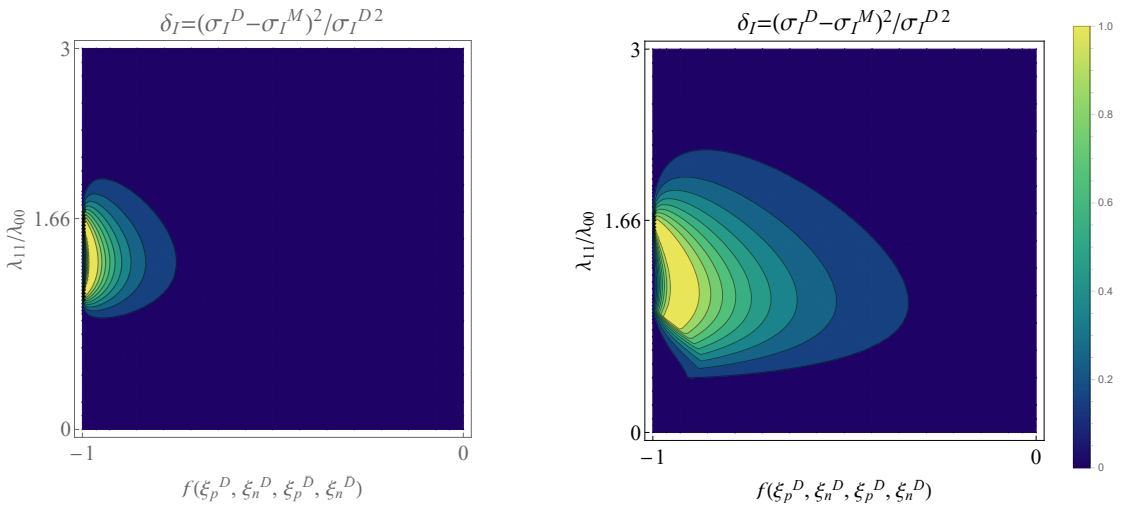

Figure 5.1: The discrimination quantity δ_I for iodine in the experimental ensemble {I, Na, F} is shown to the left. To the right δ_I for the mock setup {I, Fake, F} is shown, where the value of $\sqrt{S_{00}/S_{11}}$ for the mock target Fake has been chosen to be 1/3. The difference in δ_I is seen in the difference in size of the coloured regions.

A comparison between δ_I was also made between {I, Na, F} and the targets {I, Xe, Ge}, where xenon (Xe) and germanium (Ge) has values $\sqrt{S_{00}/S_{11}} = 0.70$ and 0.78. The result is shown in Figure 5.2.

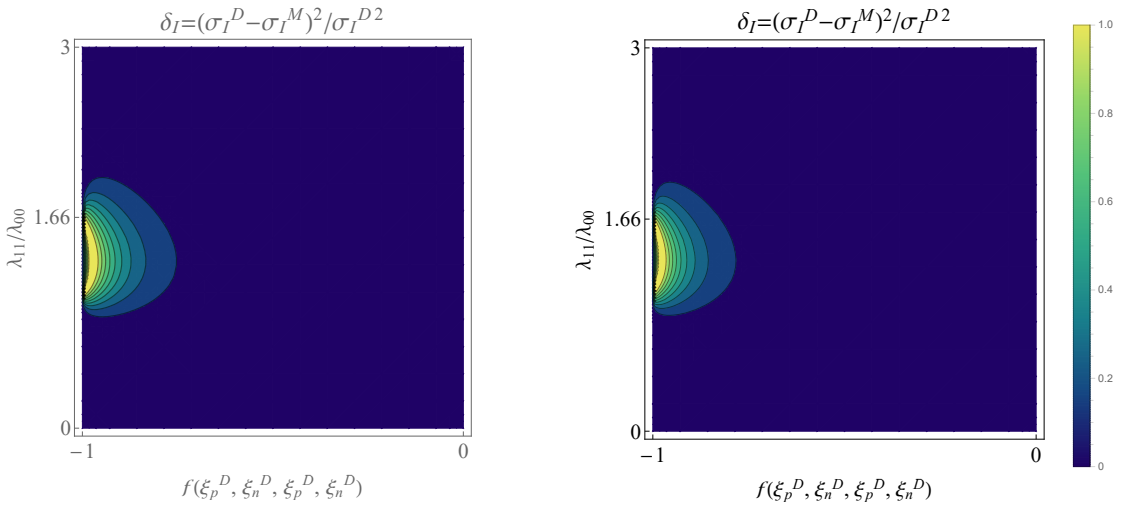

Figure 5.2: The δ_I value for iodine in the experimental ensembles {I, Na, F} (to the left) and {I, Xe, Ge} (to the right). The region in parameter space where discrimination can be made between Dirac and Majorana is shown in colour, where a brighter colour implies better circumstance for discrimination. A very slight difference in the size of these regions appears.

Finally, in order to investigate the effect of having cancellation in one of two targets with close values of $\sqrt{S_{00}/S_{11}}$, δ_F and δ_{Na} are compared for the setup {I, Na, F} in Figure 5.3.

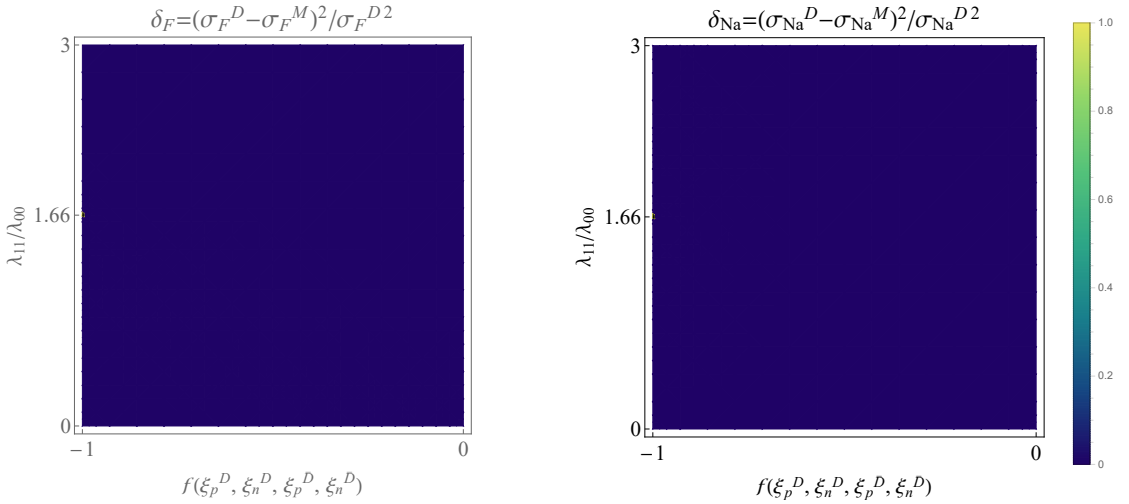

Figure 5.3: The δ_F-value for fluoride in the experimental ensemble {I, Na, F} is shown to the left. The δ_{Na}-value for sodium in the same experimental setup is shown to the right. The region in parameter space where discrimination can be made between Dirac and Majorana is shown in colour, where a brighter colour implies better circumstance for discrimination. No such region is observed here, due to the similar value of $\sqrt{S_{00}/S_{11}}$ for the two targets.

6
Discussion

The plots showing parameter space restrictions of discrimination in chapter 5 shows that, in theory, it should be possible to confirm the particle nature of a Dirac dark matter particle that interacts only via spin dependent interactions. The values of δ all agree with the theoretical predictions, both for good and bad setups for discrimination. An interesting observation can be made by comparing Figures 5.1 and 5.2. Consider the much wider region of δ-values different from 0 in Figure 5.1 due to the larger split in $\sqrt{S_{00}/S_{11}}$ values in the mock-setup. From this, one is easily lead to believe that the closer two of the three targets are in terms of $\sqrt{S_{00}/S_{11}}$ values, the region in parameter space where discrimination is possible would get smaller and smaller. While this is indeed true, there seems to be a kind of saturation of this scaling. Looking at Figure 5.2, where the difference in $\sqrt{S_{00}/S_{11}}$ between Xe and Ge is only $1.05 - 1.03 = 0.02$ compared to $1.17 - 0.96 = 0.21$ for Na and F, the discrimination area is roughly the same in both setups. This is a very useful attribute if the test were to be carried out in practice and this region of parameter space would turn out to be of interest. One could then use both the experimental setup {I, Na, F} and {I, Xe, Ge} to investigate the spin dependent discrimination.

The lack of δ_F- and δ_{Na}-regions with non-zero value in Figure 5.3 agrees with our earlier conclusion that having cancellation close to the $\sqrt{S_{00}/S_{11}}$ value of two targets might lead to a low discrimination possibility. The same result can actually be seen in the plots presented by Kavanagh et al. for the spin independent case [3], but in those cases the area of possible discrimination is just smaller, not zero. This effect would be an interesting thing to investigate further if one were to combine the two tests in some way in the future. Here, we settle for just concluding that cancellation in a third target with $\sqrt{S_{00}/S_{11}}$ very different from the other two is the best way to possibly confirm spin dependent Dirac dark matter particles within this particular framework.

It is important to note the various limitations of the test described here. First and foremost, this test is *not* designed to verify the existence of dark matter. It is entirely dependent on already having dark matter signals at hand for the targets considered. The test can then be used to investigate the particle nature of the verified dark matter particle. Apart from this, we have also seen some further constraints on the test. An especially important one is given on which parts of $\{\lambda_{11}/\lambda_{00},\, f\}$ parameter space that the test work. If the fundamental couplings that appear on Lagrangian level turns out to place the values of $\lambda_{11}/\lambda_{00}$ and f outside the close vicinity of a region where cancellation of the first term in the cross section of one of the targets takes place, the test will fail. We have also seen that the discrimination

procedure itself is not dependent on the scale of the underlying particle theory, i.e. under a global rescaling of the couplings to nucleons, the discrimination measure δ can still have a large value. However, the amplitude of the measured signal is obviously dependent on the values of the couplings, so discrimination might still be theoretically possible, while the actual measurements ends up falling within the background noise of the experiments for certain coupling combinations.

When constructing the differential cross section for Dirac dark matter, we based our assumption on the standard freeze-out scenario, meaning equal contribution from particles and antiparticles. If this assumption would turn out to be wrong, the Dirac differential cross section would have to be weighted to account for the correct abundance of particles and antiparticles.

We have only considered scattering operators at zero momentum transfer, and have assumed the rest to be heavily suppressed. Of course, it could turn out that higher order terms have couplings of sufficiently high order to make them important. In that case, the amplitude derived from the nucleon Lagrangian would have to be modified to account for these contributions.

No uncertainties or deviations from the astrophysical models for ρ_χ or the velocity distribution $f(v)$ have been reviewed in this work. If one were to carry out the test in practice, uncertainties of these inputs would also have to be included.

7
Conclusion

For the spin dependent theory presented within this thesis, it seems to be theoretically plausible to conclude the correct particle nature of a Dirac dark matter particle using only direct detection data. A range of target nuclei, all of which are present in current direct detection searches for dark matter, that would make this possible have been presented. They are: ^{131}Xe, ^{127}I, ^{73}Ge, ^{23}Na and ^{19}F. Other target elements, and isotopes of the ones mentioned here, are also possible candidates, as long as they have a non-zero nuclear spin and large enough differences in their values of $\sqrt{S_{00}/S_{11}}$.

A natural continuation of the work presented in this thesis would be to carry out a statistical analysis of the discrimination significance to see what amount of underlying observations would actually be needed in order to successfully discriminate between Dirac and Majorana dark matter. The foundation for this has been presented here, and turning these results into discrimination significance would be possible following the statistical procedure outlined in section 4.3.

As seen in the discussion of chapter 6, the test described in this thesis does not account for the several uncertainties that would have to be considered in order to confirm a Dirac dark matter particle in practice. It is thereby important to note that this is only a preparation study, and additional modifications are in order for future use of the results. At this point, the conclusions here presented are thus only of theoretical interest. However, they could turn out to be important if future projects take them into account when using potential dark matter discoveries to study the particle nature of dark matter.

Bibliography

[1] G. Bertone and D. Hooper. "A History of Dark Matter". arXiv:1605.04909v2 [hep-ph].

[2] C. Mosese et al. "European Astroparticle Physics Strategy 2017-2026", APPEC.

[3] B. J. Kavanagh, F. S. Queiroz, W. Rodejohann, C. E. Yaguna. "Prospects for determining the particle/antiparticle nature of WIMP dark matter with direct detection experiments". arXiv:1706.07819 [hep-ph].

[4] Bessel, F. W. (1844), MNRAS 6, 136.

[5] Hubble, E., and M. L. Humason (1931), Astrophys. J. 74, 43.

[6] Zwicky, F. (1933), Helvetica Physica Acta 6, 110.

[7] J.A. Tyson, G.P. Kochanski and I.P. Dell'Antonio, Astrophys. J. Lett. 498 (1998) 107

[8] M. S. Roberts and A. H. Rots (1973), A&A 26, 483.

[9] D. H. Rogstad and G. S. Shostak (1972), Astrophys. J. 176, 315.

[10] Babcock, H. W. (1939), Lick Observatory Bulletin 19, 41.

[11] M. Milgrom. "MOND–a pedagogical review". arXiv:astro-ph/0112069v1.

[12] M. D. Leo. "Rotation curve of spiral galaxy Messier 33 (Triangulum)", CC BY-SA 4.0. URL: `https://creativecommons.org/licenses/by-sa/4.0`

[13] D. Clowe et al. "A DIRECT EMPIRICAL PROOF OF THE EXISTENCE OF DARK MATTER". arXiv:astro-ph/0608407.

[14] A. Robertson et al. "What does the Bullet Cluster tell us about self-interacting dark matter?". arXiv:1605.04307v2 [astro-ph.CO].

[15] NASA/CXC/M. Weiss "Composite image showing the galaxy cluster 1E 0657-56". URL: `https://upload.wikimedia.org/wikipedia/commons/a/a8/1e0657_scale.jpg`

[16] G. Bertone, D. Hooper and J. Silk. "Particle Dark Matter: Evidence, Candidates and Constraints". arXiv:0404175v2 [hep-ph].

[17] S. Weinberg. "Cosmology". Oxford: Oxford University Press, 2008. isbn: 0191523607;9780191523601;9780198526827;0198526822.

[18] Planck Collaboration: P. A. R. Ade et al. "Planck 2015 results. XIII. Cosmological parameters". arXiv:1502.01589 [hep-ph].

[19] D. J. Fixsen. "THE TEMPERATURE OF THE COSMIC MICROWAVE BACKGROUND". arXiv:0911.1955 [hep-ph].

[20] W. Hu. "Wandering in the Background: A Cosmic Microwave Background Explorer". arXiv:astro-ph/9508126.

[21] ESA and the Planck Collaboration. "Planck Power Spectrum". URL: `http://www.esa.int/spaceinimages/Images/2013/03/Planck_Power_Spectrum`

[22] C. Sivaram and K. Arun. “Some more Exotic Dark Matter Candidates: GUT Balls, Fermi Balls. . . ”. arXiv:1109.5266 [physics.gen-ph].
[23] S. P. Martin. “A Supersymmetry Primer”. World Scientific Publishing Co, 1998.
[24] G. Servant, T. M.P. Tait. “Is the Lightest Kaluza-Klein Particle a Viable Dark Matter Candidate?”. arXiv:hep-ph/0206071v2.
[25] R. Bernabei et al. “Final model independent result of DAMA/LIBRA-phase1”. arXiv:1308.5109.
[26] M. Drewes. “The Phenomenology of Right Handed Neutrinos”. arXiv:1303.6912 [hep-ph].
[27] S. Dodelson and L. M. Widrow. “Sterile neutrinos as dark matter”, Physical Review Letters, 72:17–20, January 1994.
[28] L. J. Rosenberg and K. A. van Bibber, Phys. Rept. 325 (2000) 1.
[29] I. G. Irastorza, J. Redondo. “New experimental approaches in the search for axion-like particles”. arXiv:1801.08127 [hep-ph].
[30] D. Green, P. D. Meerburg, J. Meyers. “Aspects of Dark Matter Annihilation in Cosmology”. arXiv:1804.01055 [astro-ph.CO].
[31] The ATLAS Collaboration, G Aad, et al. “The ATLAS experiment at the CERN Large Hadron Collider”, Journal of Instrumentation, 3(08):S08003, 2008.
[32] XENON100 Collaboration: E. Aprile. “XENON100 Dark Matter Results from a Combination of 477 Live Days”. arXiv:1609.06154 [astro-ph.CO].
[33] M. W. Goodman and E. Witten. “Detectability of certain dark-matter candidates”. Physical Review D, 31:3059–3063, Jun 1985
[34] T. M. Undagoitia, L. Rauch “Dark matter direct-detection experiments”. arXiv:1509.08767v2 [physics.ins-det].
[35] J.D. Lewin, RF. Smith “Review of mathematics, numerical factors, and corrections for dark matter experiments based on elastic nuclear recoil”. Astroparticle Physics 6 (1996) 87-112
[36] J. I. Read. “The Local Dark Matter Density ”. J. Phys. G41, 063101 (2014). arXiv:1404.1938 [astro-ph.GA].
[37] A. H. G. Peter, V. Gluscevic, A. M. Green, B. J. Kavanagh, and S. K. Lee. “WIMP physics with ensembles of direct-detection experiments”, Phys. Dark Univ. 5-6, 45 (2014). arXiv:1310.7039 [astro-ph.GA]
[38] M. Feast and P. Whitelock. “Galactic Kinematics of Cepheids from Hipparcos Proper Motions”, Mon. Not. Roy. Astron. Soc. 291, 683 (1997). arXiv:astro-ph/9706293 [astro-ph]
[39] J. Bovy et al. “THE MILKY WAY’S CIRCULAR VELOCITY CURVE BETWEEN 4 AND 14 KPC FROM APOGEE DATA”, Astrophys. J. 759, 131 (2012). arXiv:1209.0759 [astro-ph.GA]
[40] C. McCabe. “The Earth’s velocity for direct detection experiments”, JCAP 1402, 027 (2014). arXiv:1312.1355 [astro-ph.CO]
[41] M. C. Smith et al. “The RAVE Survey: Constraining the Local Galactic Escape Speed”, Mon. Not. Roy. Astron. Soc. 379, 755 (2007). arXiv:astro-ph/0611671 [astro-ph]
[42] T. Piffl et al. “The RAVE survey: the Galactic escape speed and the mass of the Milky Way”, Astron. Astrophys. 562, A91 (2014). arXiv:1309.4293 [astro-ph.GA]

[43] M. E. Peskin and D. V. Schroeder. “An Introduction to Quantum Field Theory”. Westview Press, 1995.
[44] A. L. Fitzpatrick, W. Haxton, E. Katz, N. Lubbers, and Y. Xu. “The effective field theory of dark matter direct detection”. Journal of Cosmology and Astroparticle Physics, 2:004, February 2013.
[45] N. Anand, A. L. Fitzpatrick, W. C. Haxton “Model-independent WIMP Scattering Responses and Event Rates: A Mathematica Package for Experimental Analysis”. arXiv:1308.6288 [hep-ph].
[46] R. Catena and B. Schwabe. “Form factors for dark matter capture by the Sun in effective theories”. arXiv:1501.03729 [hep-ph].
[47] G. Bélanger et al. “Dark matter direct detection rate in a generic model with micrOMEGAs 2.2”. arXiv:0803.2360 [hep-ph].
[48] E. Del Nobile et al. “Tools for model-independent bounds in direct dark matter searches”. arXiv:arXiv:1307.5955v5 [hep-ph].
[49] A. L. Fitzpatrick et al. “The Effective Field Theory of Dark Matter Direct Detection”. arXiv:1203.3542 [hep-ph].
[50] E. W. Kolb and M. S. Turner. Front. Phys. 69, 1 (1990).
[51] C. E. Yaguna, “New Constraints on Xenonphobic Dark Matter from DEAP-3600”. arXiv:1902.10256 [hep-ph].
[52] XENON Collaboration: E. Aprile et al. “The XENON1T Dark Matter Experiment”. arXiv:1708.07051 [astro-ph.IM].
[53] G. Cowan, K. Cranmer, E. Gross, and O. Vitells. “Asymptotic formulae for likelihood-based tests of new physics”, Eur. Phys. J. C71, 1554 (2011), [Erratum: Eur. Phys. J.C73,2501(2013)]. arXiv:1007.1727 [physics.data-an]